Jour. Fac., Sci., Hokkaido Univ., Ser. IV,
vol. 21, no. 2, Sept., 1984, pp. 197-250.

PETROLOGY OF THE HOROMAN ULTRAMAFIC ROCKS IN THE HIDAKA METAMORPHIC BELT, HOKKAIDO, JAPAN

by

Kiyoaki Niida

(with 36 text-figures and 7 tables)

Abstract

The Horoman ultramafic massif, covering more than 8×10 km in the Hidaka Metamorphic Belt, is an "alpine-type" peridotite which is a gently warped sheet about 3,000 m in thickness. The massif exhibits a conspicuous layered structure which consists of layers of dunite, lherzolite, plagioclase lherzolite, and a small amount of gabbro and pyroxenite.

Coexisting minerals from all the rock types of the layered ultramafic to mafic sequence were analysed by EPMA. The ferromagnesian minerals show large compositional variations in accordance with lithological change in the series of dunite → lherzolite → plagioclase lherzolite → gabbro. Forsterite content of olivine varies successively from $Fo_{92.5}$ to $Fo_{64.5}$. Enstatite content of orthopyroxene also varies from $En_{93.0}$ to $En_{85.5}$. Large and continuous compositional variation was also obtained for clinopyroxenes, e.g. $Ca_{46}Mg_{51}Fe_3$ from dunite, $Ca_{48}Mg_{48}Fe_4$ from lherzolite, $Ca_{49}Mg_{46}Fe_5$ from plagioclase lherzolite, $Ca_{50}Mg_{44}Fe_6$ from the margin of gabbro, and $Ca_{38}Mg_{39}Fe_{23}$ from the center of gabbro. Al and Ti contents of clinopyroxenes and pargasitic amphiboles increase with decrease of the Mg/ Mg + Fe ratio. The mineralogical characteristics indicate that the Horoman layered sequence represents a magmatic series formed by fractional crystallization. The gabbroic seams in the plagioclase lherzolite and the layers of gabbro were probably formed by crystallization of residual liquid which were slightly alkaline in chemical nature.

The Horoman ultramafic rocks are strongly modified by deep-seated deformation and recrystallization, and additionally by mylonitization during the up-thrusting intrusion into the Earth's crust. The primary composition of minerals, obtained by step-scanning EPMA analyses, are recognized as a distinct and uniform compositional plateaus at the cores of large, porphyroclastic, primary grains. The equilibration temperatures were calculated for the orthopyroxene-clinopyroxene pairs of primary porphyroclasts, using the Opx-Cpx geothermometer. The temperatures range from 900°C to 1,100°C. The estimates for the neoblastic pyroxene pairs are slightly lower, ranging between 850°C and 1,000°C. The rocks might have re-equilibrated under the subsolidus conditions in the upper mantle.

Introduction

The Horoman ultramafic massif situated at the southwestern end of the Hidaka Metamorphic Belt crops out over approximately 8×10 km. The massif is representative of "alpine-type" peridotite intrusions with conspicuous layered structure.

Subsequent to the pioneer works on the general geology of this area by Yamane (1911), Ohdaira (1926), and Takeuchi (1937), a detailed study of the Horoman massif was carried out by Hunahashi (1941), and later by Igi (1953). Both authors described the general geology and petrography of the massif and commented briefly on its structure. A geologic map including this massif was published by Hunahashi and Igi (1956) with an explanatory text ("Horoizumi" sheet, scale 1:50,000). A more detailed geologic map of the southern central part of the massif with some petrographic descrip-

Contribution from the Department of Geology and Mineralogy, Faculty of Science, Hokkaido University, No. 1834.

tions was published by Harada et al. (1960). Petrography of the main rock types of the massif was studied by Komatsu and Nochi (1966).

After the above works, the origin and mode of emplacement of the Horoman massif have been discussed. Nagasaki (1962, 1966) considered that the Horoman body was formed by successive "hot" intrusions of liquid magma and its crystallization differentiation in situ. His descriptions of the layering, however, are inadequate and contain some misunderstandings as pointed by Komatsu and Nochi (1966). On the basis of mineralogical data Onuki (1965) suggested that the Horoman massif crystallized under higher temperatures and slightly higher pressures than other "alpine-type" peridotite intrusions, but he did not determine whether this massif intruded in a liquid or solid state. Komatsu (1970) suggested that the genesis of fine-grained parts in the ultramafic rocks can be explained by crystallization from the residual liquid. Subsequently, Tazaki et al. (1972) carried out an experimental study on pyroxene-spinel symplectites from the Horoman lherzolite. Although many arguments have been made as mentioned above, important problems such as primary crystallization, subsolidus recrystallization and re-equilibration, and mode of emplacement of the Horoman ultramafic massif have been left unsolved.

Recently, equilibration condition has been able to be evaluated by using various geobarometers and geothermometers, and then pressure and temperature paths for "alpine-type" peridotites from many orogenic belts have been estimated (e.g. Ernst, 1978; Shervais, 1979; Obata, 1980). Primary condition as shown by compositional zoning in porphyroclastic-primary grains has been also recognized. However, primary-magmatic process such as fractional crystallization and partial melting for peridotites from the upper mantle, have not yet been discussed adequately.

This paper deals with petrography, mineral chemistry, petrochemistry, and structural and textural petrology of the Horoman ultramafic rocks, and then provides some important petrologic constraints on the nature and tectonic history of the intrusion.

Geology

Seven major masses of "alpine-type" peridotite are distributed along the western side of the Hidaka Metamorphic Belt (Hunahashi and Hashimoto, 1951; Hunahashi, 1957; Hashimoto, 1947, 1975; Nochi and Komatsu, 1967; R.G.P.I., 1967).

The Hidaka Metamorphic Belt consists of two zones, as shown in Text-fig. 1. One is the Western Zone characterized by metaophiolite, which is composed mainly of ultramafic tectonite, metamorphosed ultramafic to mafic cumulate and massive gabbro, amphibolite, greenschist, and minor amounts of pelitic schist (Miyashita, 1983). The other is the Main Zone, which is composed of the Lower and Upper metamorphic sequences. In the Lower metamorphic sequence granulite and amphibolite show a regular arrangement, whereas in the Upper sequence biotite gneiss and schist are intruded by migmatites and granites. According to Osanai et al. (1981), the Main Zone is divided into five metamorphic zones; I) chlorite + muscovite, II) muscovite + biotite, III) biotite + sillimanite + garnet + K-feldspar, IV) garnet + biotite + cordierite + K-

feldspar, and V) garnet + orthopyroxene + cordierite + K-feldspar. A large amount of gabbro intruded into the Main Zone and disturbed the above arrangement.

The Geological setting of the Hidaka Metamorphic Belt and its nature are discussed summarily by Komatsu et al. (1983). The Western Zone of the Hidaka Metamorphic Belt is regarded as an ancient oceanic crust (Miyashita and Maeda, 1978), whereas the Main Zone represents a crustal section of continent or island arc (Komatsu et al., 1981; Osanai et al., 1981). The "alpine-type" peridotite masses are exposed along the fault zone just between the Western and the Main Zones of the Hidaka Metamorphic Belt (Text-fig. 1). Rock types of the peridotites from the Hidaka Metamorphic Belt are summarized by Niida and Katoh (1978). L-series (lherzolite series) showing a conspicuous layering occurs along the above boundary zone at Uenzaru, Pankenushi, Menashibetsu, Horoman, Pon-Nikanbetsu, Nikanbetsu, and Abeyaki, from north to south. H-series (harzburgite series) of ultramafic tectonites occurs at Uenzaru, Tottabetsu, Oku-Niikappu, and Koibokushu-Shibichari. The Horoman ultramafic massif is situated at the southwestern extremity of the Hidaka Metamorphic Belt as shown in Text-fig. 1. Apoi-dake (810.6 m) and adjacent areas in the Horoman region are composed of ultramafic rocks, banded biotite gneiss, schistose biotite hornfels, schistose amphibolite and various kinds of gabbro. The Horoman massif is located at the geological position between the Western Zone and the Main Zone of the Hidaka

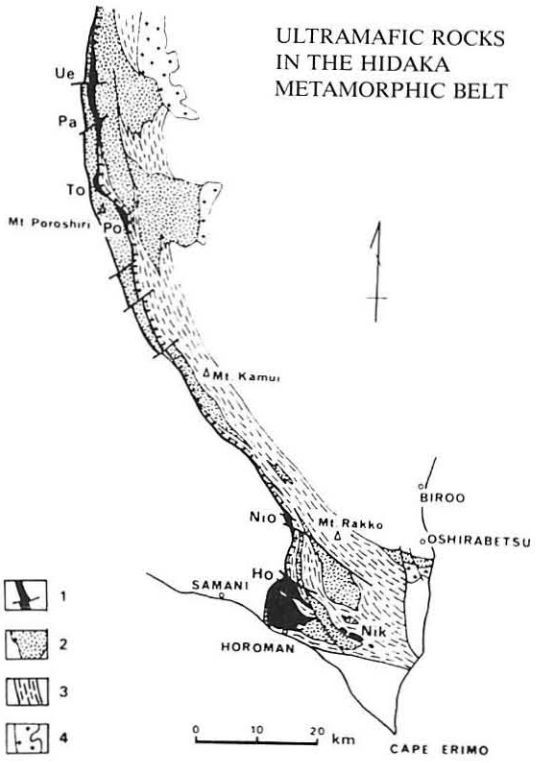

Text-fig. 1 Map showing distribution of the ultramafic rocks in the Hidaka Metamorphic Belt
1. ultramafic rocks. 2. mafic rocks (metaophiolite and gabbros). 3. metamorphic rocks (Px-gneiss, Bi-gneiss and migmatite). 4. granitic rocks. Ue: Uenzaru. Pa: Pankenushi. To: Tottabetsu. Po: Poroshiri. Nio: Niobetsu. Ho: Horoman. Nik: Nikanbetsu.

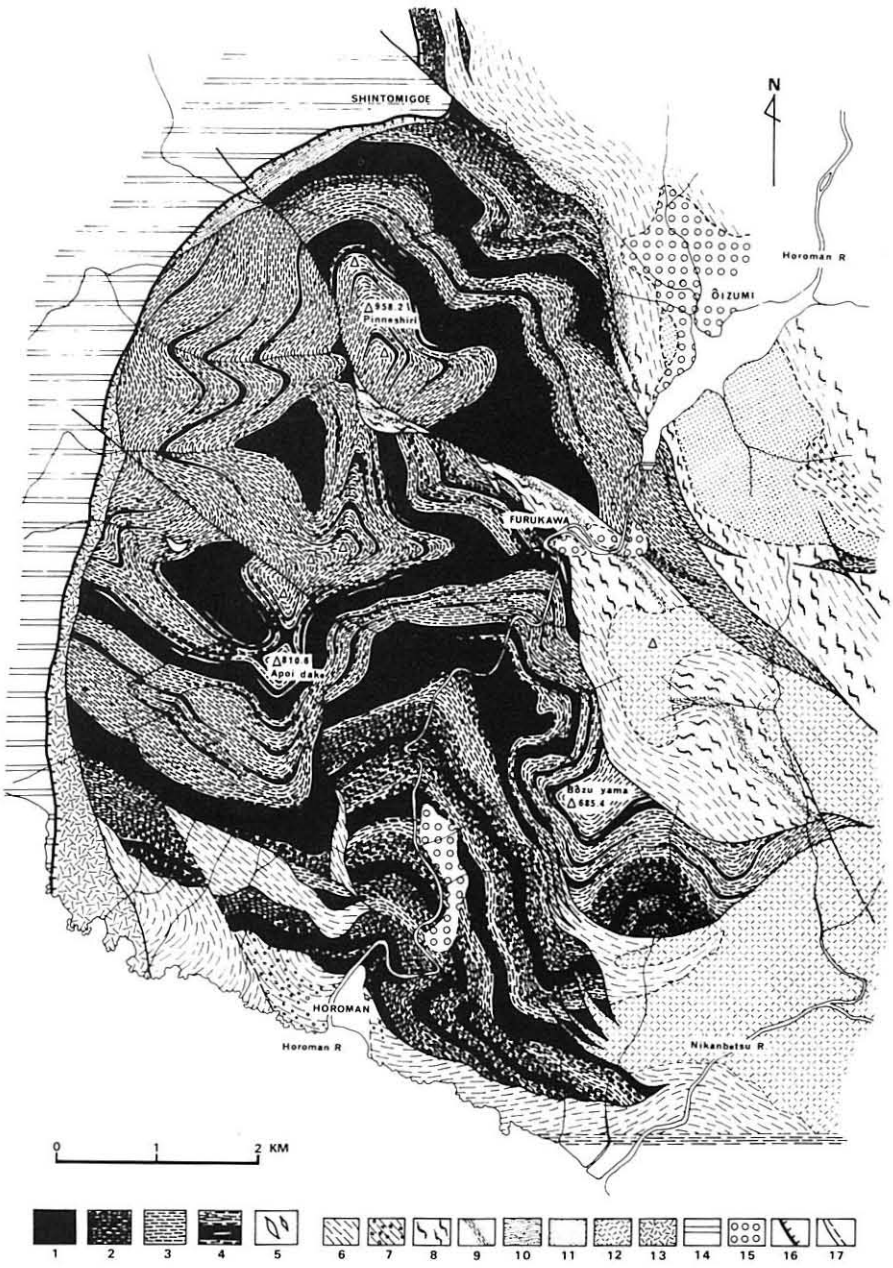

Text-fig. 2 Geologic map of the Horoman region
1. dunite 2. lherzolite 3. plagioclase lherzolite 4. gabbro 5. pegmatite 6. schistose biotite hornfels 7. plagioclase porphyroblastic biotite schist 8. biotite gneiss 9. schistose amphibolite 10. greenschist and blackschist 11. diorite 12. gabbro 13. saussurite gabbro 14. Hidaka Super Group 15. alluvium 16. thrust fault 17. fault and shear zone

Metamorphic Belt.

The Horoman ultramafic massif crops out over approximately 8 × 10 km (Text-fig. 2) and is more than 3,000 m in thickness. To the west the Horoman massif is bordered by a thrust fault zone involving meta-gabbro, greenschist and blackschist, which constitute metaophiolite of the Western Zone, and contact with non-metamorphosed sedimentary rocks of the Pre-Cretaceous Hidaka Super Group (Minato et al., 1965). The eastern and northern margins of the massif are irregularly bounded by NW-SE striking faults and shear zones. Along the strongest shear zone, near Furukawa, wedge-shaped masses of banded gneiss and amphibolite occur in a form of "septum" faulted within the ultramafic rocks. Evidence of contact metamorphism has not been found around the massif.

Serpentinization is usually developed at the margin of the massif and along faults and shear zones. However, the major part of the massif is extremely fresh, though in parts it is weakly serpentinized.

Petrography

The ultramafic rocks of the Horoman massif are made up almost entirely of olivine, orthopyroxene, and clinopyroxene. Plagioclase, spinel, and amphibole are important minor constituents. The Horoman massif exhibits well developed compositional layering which consists of layers of the following rock types.

The ultramafic type, which constitutes more than 95% of the Horoman massif, comprises dunite (D), harzburgite (H), lherzolite (L), plagioclase lherzolite (Pl I and Pl II), orthopyroxenite (OPX) and clinopyroxenite (CPX). Dunite, lherzolite, and plagioclase lherzolite are representatives of the Horoman layered massif. Text-fig. 3 shows their mineral assemblage and modal composition. As clearly shown in the modal variation diagram (Text-fig. 4), dunite gradually changes into lherzolite. Most of harzburgite occurs as an intermediate type between dunite and lherzolite. In the field observation it is difficult to distinguish harzburgite from dunite.

The gabbroic rocks occur as gabbro I (GB I) and gabbro II (GB II) layers in the ultramafic rocks. Besides, a small amount of gabbro occurs as seams in plagioclase lherzolite I and II. Wide variations in modal composition are recognized in the layers of gabbro I and II from the center to the margin as shown in Text-fig. 5.

The Horoman massif is divided into the Lower Zone (about 2,000 m in thickness)

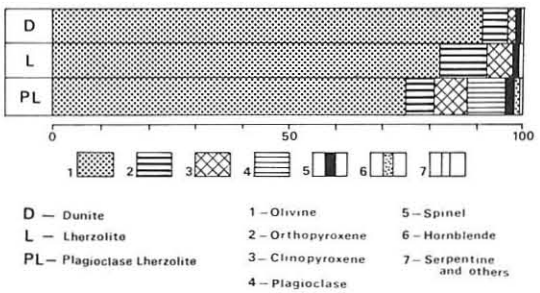

Text-fig. 3 Modal composition of the three representative rocks in the ultramafic series

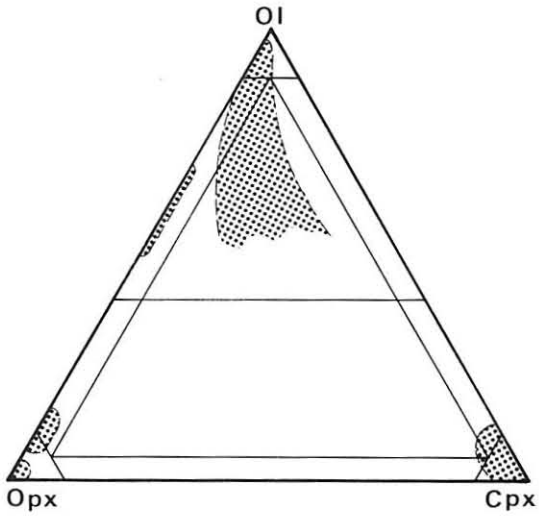

Text-fig. 4 Plot of the ultramafic rocks from the Horoman massif on the Ol-Opx-Cpx diagram for classification of ultramafic rocks (IUGS, 1973)

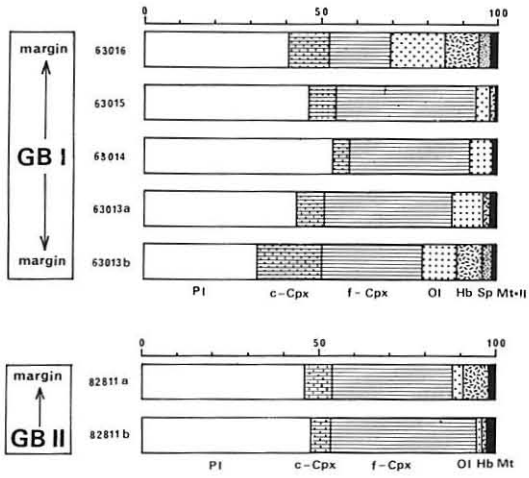

Text-fig. 5 Modal variation in the gabbroic layers (GB I and GB II) from the center to the margin

and the Upper Zone (more than 1,000 m). In the Lower Zone, the main rock types of dunite, lherzolite and plagioclase lherzolite are predominant. On the other hand, in the Upper Zone gabbros are characteristic rocks. All rock types from the Horoman massif with their mineral assemblages are summarized in Table 1.

DUNITE

Dunite occurs mainly in the Lower Zone of the massif, though it is also found in the Upper Zone. Thick layers of dunite, about 250 m in maximum thickness, appear five times in the Lower Zone. Besides, numerous thin layers of dunite ranging from a few centimeters to several meters in thickness occur commonly in plagioclase lherzolite of

Table 1 Mineral assemblages in the Horoman ultramafic to mafic rocks

ROCK TYPE	ULTRAMAFIC	GABBROIC
D	Ol + Opx + Sp + (Cpx)	
L	Ol + Opx + Cpx + (Sp)	
Pl I	Ol + Opx + Cpx ———	Pl + br.Sp + Ol + Cpx* + (Ti-parg)
Pl II	Ol + Opx + Cpx ———	Pl + gr.Sp + Cpx** + Ol + Ti-parg
GB I	——— margin:	Pl + gr.Sp + Cpx** + Ol + Ti-parg∿Kaer
	center:	Pl + Il∿Mt + Cpx*** + Ol
GB II	———	Pl + Mt + Cpx* + Parg + Ol
OPX	Opx + (Ol + Cpx + Pl)	
CPX	Cpx + (Ol + Opx + Pl)	

Ol: olivine Opx: orthopyroxe Il: ilmenite Sp: spinel Cpx: clinopyroxene
Mt: magnetite Pl: plagioclase Ti-parg: titaniferous pargasite Kaer: kaersutite
parg: pargasite
*diopside **titaniferous diopside∿salite ***salite∿calsic augite
( ) minor minerals

both the Upper and Lower Zones. The dunite is easily recognizable by its yellowish-brown color due to weathering. Most of the constituent minerals are easily distinguishable on the fresh surface, i.e. yellowish-green olivine, yellowish-brown orthopyroxene, light green clinopyroxene, and black spinel. Dunite consists of 90% to 95% (volume percent) olivine ($Fo_{92.5-91.0}$), 5% to 8% orthopyroxene ($En_{92.4-91.5}$), 1% to 3% clinopyroxene ($Ca_{46}Mg_{51}Fe_3$), and approximately 1% chromian spinel.

At several localities layers of harzburgitic dunite carrying large orthopyroxene crystals are found. Near the transitional zones between dunite and lherzolite in the Lower Zone, the dunite characteristically grades into harzburgite. In some cases, harzburgite lenses, several centimeters in thickness and containing up to 50% of orthopyroxene, are interlayered within dunite. Orthopyroxenite lenses are rarely found in the dunite layer.

Spinel rich dunite layers, about 15 m in thickness and containing large crystals of spindle-shaped brown spinel, are also found in the dunite.

Olivine in the dunite varies in grain size and shape. Coarse grains, 0.4 to 5.0 mm in size, are abundant in the Lower Zone of the massif. Commonly they have irregular and interlocking grain boundaries. Undulatory extinction and kink bands in the olivine are characteristic features. Elongation of the coarse olivine grains is essentially parallel to the layering. Small grains, less than 0.4 mm in size, are commonly found in fine-grained parts of the dunite, and polygonal grains occur in the interstices between the coarse grains.

Orthopyroxene crystals are usually anhedral and coarser than olivine and clinopyroxene in the dunite. Aggregations of clinopyroxene and of brown spinel form thin layers parallel to the layering. Large, spindle-shaped brown spinels, 3-5 mm in size, occur commonly as anhedral grains disseminated throughout the dunite.

LHERZOLITE

Lherzolite contains 70% to 90% olivine ($Fo_{91.5-90.5}$), 10% to 20% orthopyroxene ($En_{91.9-90.6}$), 5% to 10% clinopyroxene ($Ca_{48}Mg_{48}Fe_4$), and about 2% spinel. On the weathered surface, the lherzolite is reddish brown and the constituent minerals are easily distinguished by their own colors, greenish-grey olivine, brown orthopyroxene, and emerald green clinopyroxene. The lherzolite occurs as a gradational layer between dunite and plagioclase lherzolite in the Lower Zone of the massif. The thickness of the lherzolite layer reaches about 200 m. No lherzolite is found in the Upper Zone. Accordingly, distribution of lherzolite is restricted within the areas along the Horoman and Sarushunai Rivers and near the Shintomigoe.

Some of lherzolite contain brownish-purple seams composed of orthopyroxene and spinel with a small amount of clinopyroxene and olivine, which are parallel to the layering. These seams, however, are not always found in the lherzolite. There are many symplectites in these seams. Two types of symplectite are distinguished; one is orthopyroxene-clinopyroxene-spinel and the other is orthopyroxene-clinopyroxene-plagioclase-spinel. Spinels are generally contained in these seams, though large "spindle"-shaped crystals of spinel are rarely found in other parts of lherzolite.

PLAGIOCLASE LHERZOLITE

Plagioclase lherzolite consists mainly of olivine ($Fo_{91.0-88.8}$), orthopyroxene ($En_{90.6-89.3}$), clinopyroxene ($Ca_{49}Mg_{46}Fe_5$), and plagioclase (An_{79-58}), with accessory brown or green spinel and pale brown Ti-pargasite. Modal plagioclase is commonly less than 15% and olivine less than 80%. The plagioclase lherzolite is common in the Upper Zone of the massif, though it also occurs in the Lower Zone.

Plagioclase usually occurs in seams associated with spinel and small amounts of olivine, clinopyroxene, and Ti-pargasite. These seams are fine grained and have characteristics of gabbroic facies. They are aligned nearly parallel to the layering. Two types of gabbroic seams are found in the plagioclase lherzolite; one composed of small aggregations of fine grained plagioclase and brown spinel (Type I), and the other thicker seams made up of coarse grained plagioclase and green spinel (Type II). The large seams of Type II grade into thin bands of gabbro (GB I), and occur mainly in the Upper Zone. The plagioclase lherzolite including type I seams is called plagioclase lherzolite I (PL I), and that composed of type II seams plagioclase lherzolite II (PL II). Deformation of olivine grains in plagioclase lherzolite is weaker than those in dunite and lherzolite. Polygonal grains of olivine are also larger in grain size. Pale brown Ti-pargasite reaches about 3% in modal composition and is included in plagioclase-rich gabbroic seams or clinopyroxene-rich parts. Ti-pargasite, however, is not always found in plagioclase lherzolite.

GABBRO

In the Upper Zone of the Horoman massif, a small amount of gabbro occurs as thin bands and layers which are interlayered with dunite and plagioclase lherzolite. Gabbroic bands are rarely found in the plagioclase lherzolite of the Lower Zone. These gabbroic bands or layers vary from a few centimeters to several meters in thickness, and are traceable for more than several meters to a few hundred meters.

There are at least two types of gabbroic layers which are different in mineralogy. The first type, gabbro I (GB I), which is the most common, consists of plagioclase (An_{86-55}), clinopyroxene ($Ca_{50}Mg_{44}Fe_6$-$Ca_{38}Mg_{39}Fe_{23}$), olivine ($Fo_{82.3-64.6}$), kaersutite and Ti-pargasite, and a small amount of green spinel, ilmenite and magnetite. This type is characterized by the presence of Ti-rich minerals such as titaniferous diopside-titaniferous salite, kaersutite, Ti-pargasite and ilmenite. The second type (GB II) consists of plagioclase (An_{90-77}), Ti-poor clinopyroxene ($Ca_{49}Mg_{45}Fe_6$-$Ca_{49}Mg_{41}Fe_{10}$), pargasite, and a small amount of olivine (Fo_{84}). This type of gabbro occurs only in the dunite from the Upper Zone. Characteristically, orthopyroxene is absent in both gabbro I and II. Some coarse grains of clinopyroxene in the gabbro I layer show a weak compositional zoning at the margin. Many small grains of clinopyroxene, olivine, kaersutite, and Ti-pargasite are accompanied with the coarse grains of clinopyroxene. Ti-rich minerals are free from the center of the gabbro I layer. Grain size of the constituent minerals becomes coarser toward the margin of the layer. No deformation texture is observed in the gabbroic rocks.

PYROXENITE

Small amounts of orthopyroxenite and clinopyroxenite occur in the Horoman massif as a compositional layer 1-30 cm thick. Orthopyroxenite is found in dunite and between dunite and gabbro I, while clinopyroxenite occurs in both dunite and plagioclase lherzolite. Orthopyroxenite usually consists of more than about 90% orthopyroxene ($En_{90.4-85.5}$), and small amounts of olivine ($Fo_{87.9}$), clinopyroxene ($Ca_{50}Mg_{45}Fe_5$), and plagioclase. On the other hand, clinopyroxenite consists mainly of clinopyroxene ($Ca_{50}Mg_{46}Fe_4$-$Ca_{47}Mg_{48}Fe_5$) with accessory olivine ($Fo_{89.3-88.9}$), orthopyroxene ($En_{89.3-89.0}$), and plagioclase.

Large lenses made up completely of magnesian orthopyroxene ($En_{92.8}$) are rarely found in a dunite layer on the western ridge of Apoi-dake, where a large single crystal of orthopyroxene attaining about 30 cm in diameter was collected.

Spinel orthopyroxenite occurs in the dunite layers and consists of up to 50% orthopyroxene, 20% to 30% brown spinel, 10% to 20% olivine, and traces of clinopyroxene, plagioclase, and pyroxene-spinel symplectite.

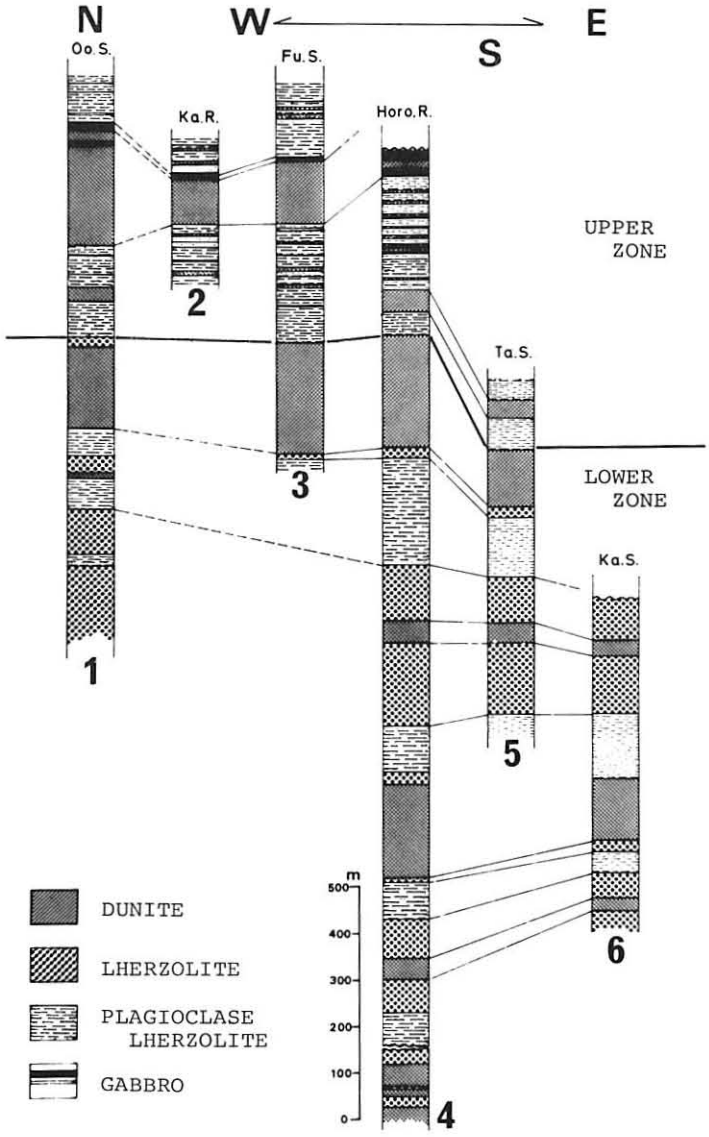

Text-fig. 6 Sections showing the rock sequences of the Horoman ultramafic massif at the following localities:
1. Oomagari-no-sawa in the northern part of the massif. 2. Western ridge of the Apoi-dake 3. Furukawa-no-sawa in the western part of the Horoman River. 4. Horoman River section, the main part of the massif. 5. Taki-no-sawa in the eastern part of the Horoman River. 6. Kage-no-sawa in the eastern part of the Horoman River.

Layering

LAYERED SEQUENCE OF THE HOROMAN MASSIF

The Horoman ultramafic massif is representative of "alpine-type" peridotites with conspicuous layered structure. The mode of layering of the Horoman ultramafic massif is clearly different from that of the layered intrusions such as Skaergaard (Wager and Brown, 1967), Stillwater (Hess, 1960), Muskox (Smith and Kapp, 1963), and others.

The Horoman massif is divided into two zones as shown in Text-fig. 6. The Lower Zone (approximately 2,000 m in thickness), which consists mainly of the ultramafic rocks of dunite, lherzolite, and plagioclase lherzolite, is well exposed along the Horoman River and in the northern part of the massif. The Upper Zone (more than 1,000 m in thickness), in which plagioclase lherzolite and gabbro develop notably, is exposed around the summits of Apoi-dake, Pinneshiri and Bozu-yama, and mainly on the western side of the massif. The lowest horizon of the exposed rocks is found at the southern end of the massif near Horoman, while the topmost is at the western end of

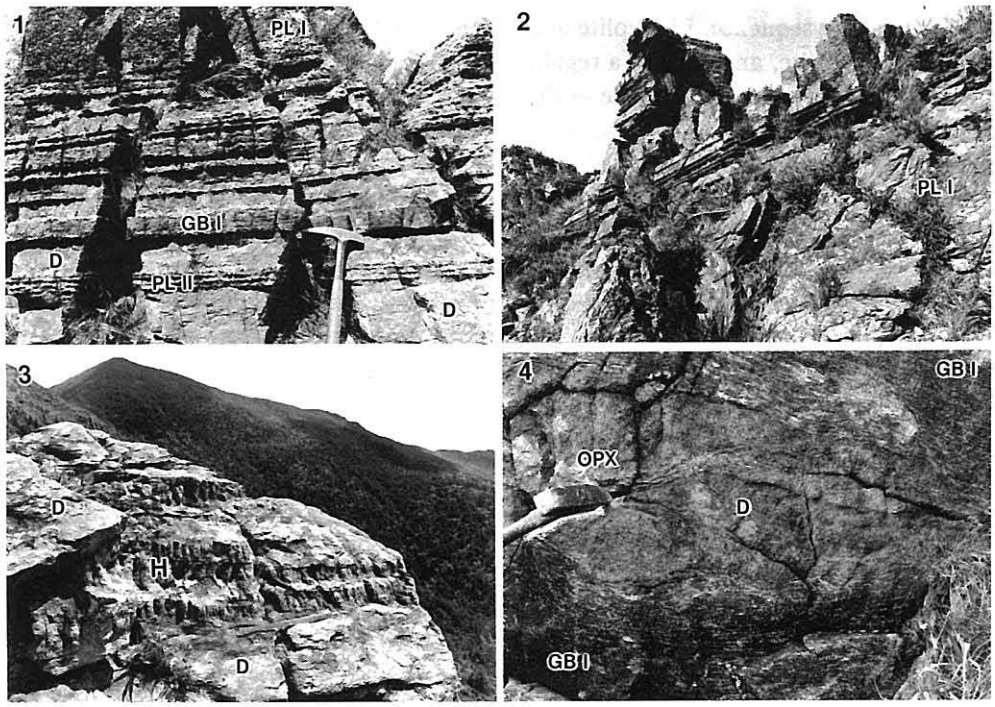

Text-fig. 7 Well-developed layered structures observed in the Upper Zone of the Horoman massif.
1 and 2. Conspicuous layering composed of layers of dunite, plagioclase lherzolite I and II, and gabbro at the northern ridge of Mt. Apoi-dake. 3. Harzburgites interlayered by dunite, at the western ridge of Mt. Apoi-dake. 4. Orthopyroxenite lens alternating with dunite and gabbro I at the western ridge of Mt. Apoi-dake.

the massif.

Two types of layering are distinguished; one is characterized by massive, thick, and gradational compositional layers in the Lower Zone of the massif, and the other is a conspicuous layered structure consisting of thin compositional layers in the Upper Zone. Hunahashi (1941), Igi (1953), and Hunahashi and Igi (1956) called the layered rocks in the Upper Zone "banded peridotites". Such conspicuous layering is shown by alternating layers of dunite, plagioclase lherzolite, and gabbro (Text-fig. 7).

Thickness of the layers in the Lower Zone varies from several tens to a few hundred meters, whereas that in the Upper Zone is considerably thinner, a few centimeters to several meters. Some of the thick layers are traceable throughout the massif as shown in Text-fig. 6. Gradational transition from one to another rock type is a characteristic feature in the Lower Zone. However, in the Upper Zone the transition is usually sharp at the contact between layers. In the Horoman massif, neither gravity stratification nor density gradation of consituent minerals within layers is found.

The predominant rock types and sequence of layering of the Lower Zone are different from those of the Upper Zone. The Lower Zone is made up mainly of the thick layers of dunite, lherzolite, and plagioclase lherzolite. Gabbro is scarcely found, except for thin gabbroic bands in the plagioclase lherzolite. The Lower Zone of the massif has a regular layering sequence. Lherzolite usually occurs between the layers of dunite and plagioclase lherzolite, and there is a regular repetition of rock types from the lower to the upper layers or vice versa; dunite → lherzolite → plagioclase lherzolite → lherzolite → dunite → ... (Text-fig. 6). The sequence of this layering type repeats at least four times in the Lower Zone as mentioned by Komatsu and Nochi (1966) and Niida (1974). It is noticed that the gradual change of rocks from dunite to plagioclase lherzolite is observed toward the lower horizon as well as toward the upper. Such "symmetrical layering" may be important in considering the genesis of the massif. Nagasaki's field observation (1966) omits the facies change toward the lower horizon.

In the Upper Zone, plagioclase lherzolite is the most predominant type, being accompanied by dunite. A small amount of gabbro and pyroxenite also occur, but no lherzolite is found. The Upper Zone of the massif is characterized by development of gabbroic rocks. Regularity of the sequence of layering as observed in the Lower Zone is not found in the Upper Zone.

LAYERING IN THE "ALPINE-TYPE" PERIDOTITES

The layering of the Horoman ultramafic massif is clearly different from that of the layered intrusions. Moreover, the layering is different from that of the zoned complexes such as Duke Island (Irvine, 1967, 1974), and Union Bay (Ruckmick and Noble, 1959) judging from the following occurrences:

1) The Horoman massif is composed mainly of layers of the ultramafic rocks, which constitute more than 95% of the whole massif.
2) Gravity stratification or density gradation is not found throughout the massif.
3) The layering can not be called "rhythmic layering" in strict sense, but "symmetrical

layering" as mentioned above.

Thayer (1960) discussed some critical differences between "alpine-type" and stratiform peridotite-gabbro complexes, and proposed a "pseudostratiform alpine-type complex" as an intermediate-type pluton, that is represented by the Bay of Island complex (Smith, 1958) in northwestern Newfoundland.

The geologic situation, partial serpentinization, cataclastic structures, and mylonitized and recrystallized textures of the Horoman ultramafic massif are similar to those of the "alpine-type" peridotites such as Dun Mountain and Red Hills (Lauder, 1965; Challis, 1965; Walcott, 1968), Twin Sisters (Ragan, 1963), Burro Mountain (Loney et al., 1971), Vulcan Peak (Himmerberg and Loney, 1973), Lizard (Green, 1964), and Alpe Arami (Möckel, 1969). The layering is reportedly not so conspicuous in these "alpine-type" peridotites. Further detailed studies should clearly distinguish the layering of the "alpine-type" peridotites from that of the layered intrusions. A similar mode of the layering to the Horoman massif can be found in the Lizard peridotite intrusion (Green, 1964). The layering in the "alpine-type" peridotites is an important aspect in considering the origin of the ultramafic intrusions.

Structure

The Horoman ultramafic massif represents an intrusion of solid mantle fragments in the form of a gently warped sheet more than 3,000 m in thickness.

Foliation planes are megascopically observed in the field by the following two features; one is a boundary plane at the top and bottom of a compositional layer, and the other is a plane formed by mineral layers as seams and aggregations.

As shown in the tectonic map (Text-fig. 8) and π-pole diagrams (Text-fig. 9), the megascopic structures of the Horoman massif are characterized by synclinal structure with an E-W axis in the central part and semi-dome structure in the southern half of the massif (Niida, 1974). The dip direction of foliation plane of layered rocks changes from east on the eastern side to west on the western side in the southern half of the massif. The dip of the layers decreases with height as observed at Apoi-dake, Bozu-yama, and other higher areas. These features indicate a dome structure for the southern half of the massif. In a more strict sense, this should be called a semi-dome structure opening to south, because the southern end of the dome is cut by a WNW-ESE trending fault. The dome structure was first described by Hunahashi (1941), and later confirmed by Igi (1953), Harada et al. (1960), and Komatsu and Nochi (1966). There is also a small dome structure at Saruchunai in the eastern part of Bozu-yama.

The northern half of the massif displays a nearly monoclinal layered structure striking roughly E-W with a moderate dip to south. A synclinal structure with an axis striking N 70°W and plunging to west is observed at the central part of the massif. Therefore, the northern part of the massif dips to the south, whereas the southern part to the north.

Liniations are observed parallel to the elongation of plagioclase + spinel seams in plagioclase lherzolite or orthopyroxene + spinel seams in lherzolite, and to the linear ar-

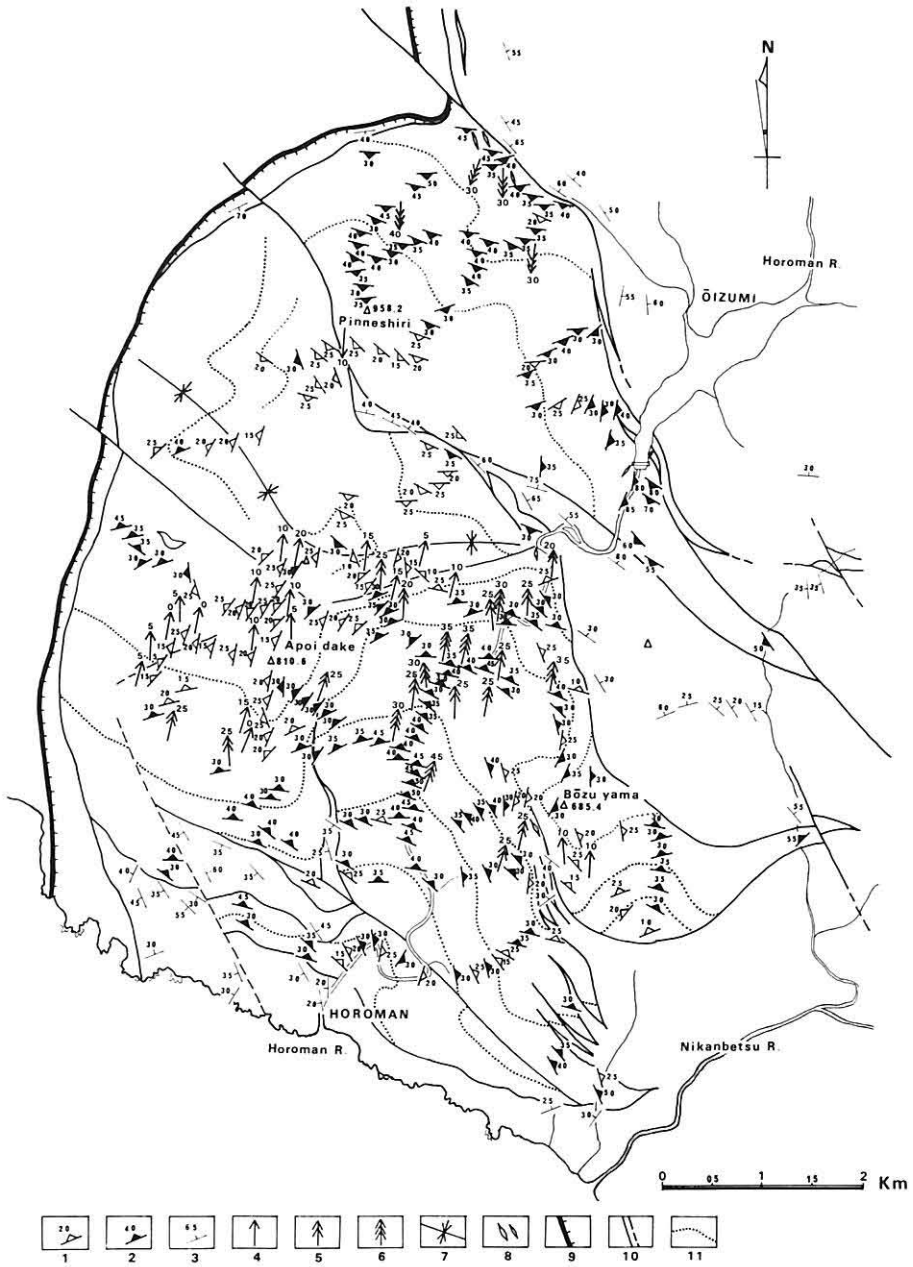

Text-fig. 8 Tectonic map of the Horoman ultramafic massif.
1. foliation (<25°), 2. foliation (≥25°), 3. schistosity and gneissosity, 4. lineation (<20°), 5. lineation (≥20°, <30°), 6. lineation (≥30°), 7. syncline, 8. pegmatite, 9. thrust fault, 10. fault and shear zone, 11. boundary of rock types.

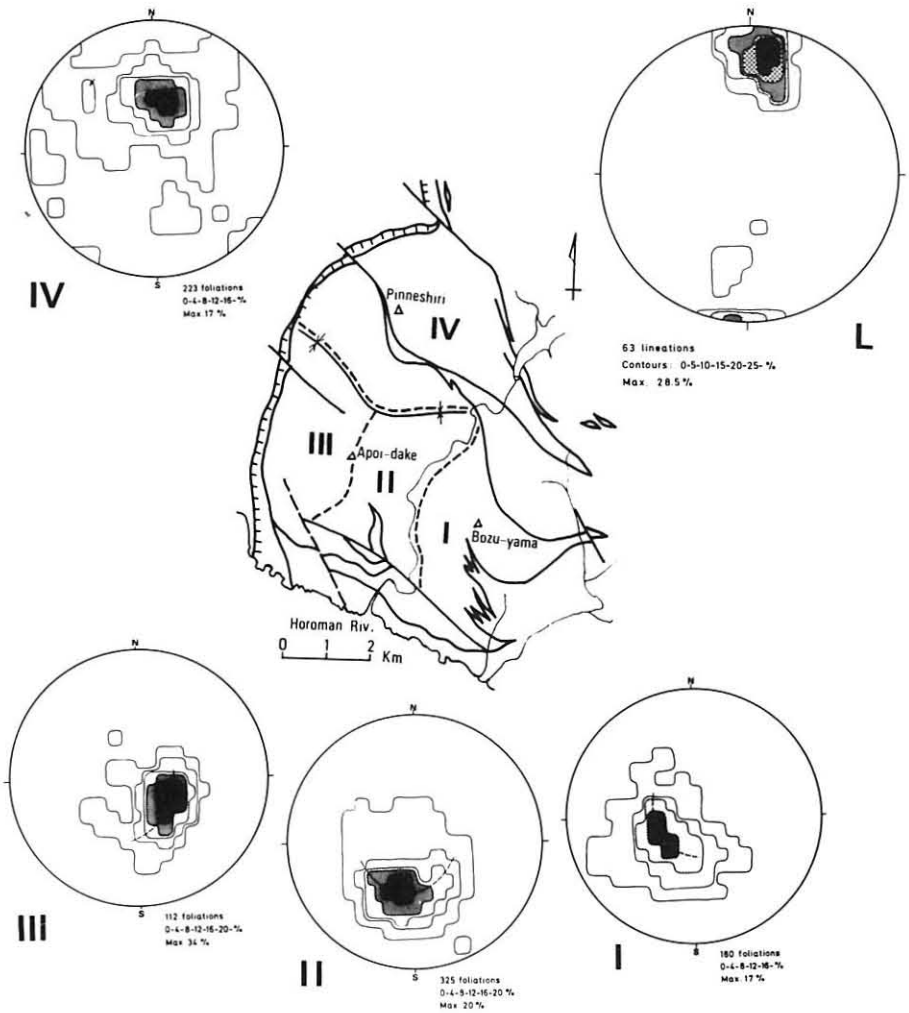

Text-fig. 9 Projection of foliations from the subareas I, II, III, and IV, and of 63 lineations throughout the massif, on the lower hemisphere of the Schmidt's net.

rangement of mineral grains such as pyroxene and spinel. The lineations have a very constant direction in about N 15°E-S 15°W throughout the massif (Text-fig. 9).

The following evidence may suggest the mode of emplacement of the Horoman massif.

1) The Horoman massif is a thick sheet in form.

2) The massif is regarded as a continuous body since the same sequences of rock types are found throughout the whole massif.

3) The massif is completely bounded by faults and shear zones. No evidence of contact metamorphism has been found.

4) Lineations throughout the massif have a constant direction of about N 15°E-

S 15°W.

5) The masses of Uenzaru and Pankenushi showing a typical sheet structure are composed of the similar rock types to the Horoman massif and occur along the same thrust fault zone on the western side of the Main Zone of the Hidaka Metamorphic Belt.

The ultramafic rocks of the massif, especially those in the Lower Zone, have mylonitic and recrystallized textures which were formed due to strong deformation.

As for the mode of emplacement of the Horoman massif, it is probable that the massif was uplifted along the deep-seated NW-SE striking thrust zone which passes through the northern side of the massif to the Pon-Nikanbetsu, Nikanbetsu, and Abeyaki ultramafic bodies. The intrusion toward the surface took place in a solid state. Strong concentration of lineations indicates that the intrusive body acted as an unbroken sheet. At the present level, the thick sheet was thrust up to the southwest with very gentle inclination. Since the northern masses of biotite gneiss and schistose amphibolite were continuously rising, the northern part of the ultramafic sheet was dragged up and dipped to the south.

Texture

Texture of the ultramafic rocks (D, L, and PL) of the Horoman massif is characterized by the coexistence of coarse- and fine-grained parts (Harada et al., 1960; Komatsu and Nochi, 1966; Niida, 1974), which appear mylonitic or recrystallized texture. No primary igneous textures are found in the ultramafic rocks except for gabbroic rocks. This texture clearly distinguishes it from layered complexes such as the Skaergaard, Stillwater and Bushveld, in which igneous cumulate textures are typically shown by olivine, pyroxene and plagioclase (Wager et al., 1960; Hess, 1960; Wager and Brown, 1967). Only the gabbroic parts (fine-grained parts of PL I & II, and GB I & II) of the Horoman massif preserve primary igneous textures.

COARSE AND FINE GRAINED PARTS

The coarse-grained parts of the ultramafic rocks are composed mainly of primary minerals of olivine, orthopyroxene, clinopyroxene and spinel. Olivine and orthopyroxene occur as porphyroclastic primary grains in the coarse parts of all rock types. Coarse grained parts containing brown spinel are recognized in dunite and are rarely found in lherzolite. Clinopyroxene in lherzolite and plagioclase lherzolite occurs also as porphyroclastic grains mainly in the coarse grained parts. Clinopyroxene in dunite, however, is found only in the fine grained parts.

The fine-grained parts typically occur as thin mineral layers ranging from 0.2 to 5.0 mm in thickness, and extend for approximately 0.5-10.0 cm^2 parallel to the layering. These thin mineral layers can be classified as follows:

1) seams of monomineralic fine olivine in all rock types,
2) seams of orthopyroxene + spinel in lherzolite,
3) seams of plagioclase + spinel in plagioclase lherzolite,

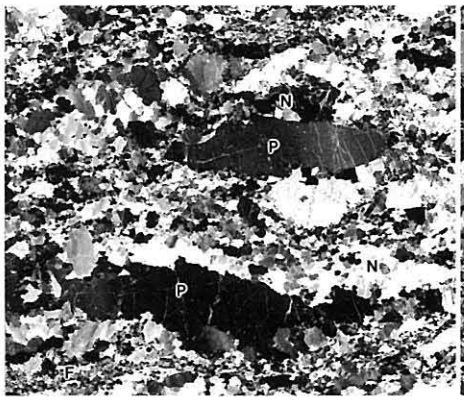

Text-fig. 10 Strongly strained and elongated olivines in plagioclase lherzolite (sample, 73629-10). P; porphyroclastic primary olivine, N; neoblastic recrystallized grain, F; fine-grained gabbroic seam.

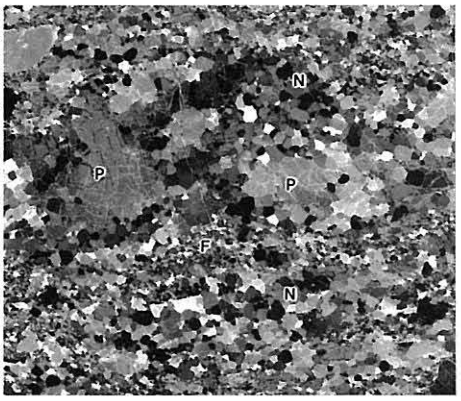

Text-fig. 11 Texture showing the coexisting relations between olivine porphyroclasts (P) and neoblasts (N), and monomineralic seams of fine grained olivine (F) in the lherzolite (sample, 71516b).

4) aggregations of clinopyroxene in dunite, and
5) aggregations of spinel in dunite.

Hirota (1955) suggested that plagioclase lherzolite of the Horoman ultramafic rocks is metamorphic because of the rare occurrence of C-twin (2-4%) in plagioclase. Tenpaku (1967) indicated that the plagioclase formed under conditions of comparatively high-temperature on the basis of the X-ray powder diffraction pattern of plagioclase. Harada et al. (1960) suggested that the fine grains of olivine were formed by granulation. More detailed descriptions of the coarse- and fine-grained parts were given by Komatsu and Nochi (1966) and Niida (1974).

THREE DIFFERENT TYPES OF OLIVINE

In the Horoman ultramafic rocks the grain size of olivine is remarkably variable. Moreover, detailed observation under the microscope showed that there are marked differences in grain shape and deformation pattern of olivine as well as grain size. Therefore, olivine grains are classified into the following three types:

1) Coarse Deformed Olivine (Porphyroclastic-Primary Olivine)

Coarse deformed olivines showing irregular boundaries and interlocking texture are usually found in the coarse grained parts of all of the rock types and texturally resemble "porphyroclasts" defined by Mercier and Nicolas (1975). In most cases grain size of olivine porphyroclasts is 0.4-5.0 mm. In the Lower Zone, especially near the lowest part of the massif, coarse grains of olivine are notably elongated by translation gliding and often exceed 5 mm length. The long axis of the deformed olivine tends to be parallel to the foliation plane. The most strained direction is usually in parallel to the lineation.

Kink bands and deformation lamellae are commonly recognized in the coarse grains of olivine as shown in Text-fig. 10. In the previous works on the Horoman ultramafic rocks, such deformation of olivine grains has not been noticed with special interest. After 1965, the slip mechanism of plastic deformation of olivine has been studied by Raleigh (1965, 1967), Carter et al. (1968), Young (1969), and Carter and AvéLallemant (1970). The slip system of the Horoman coarse deformed olivine is commonly (010) [100] (Niida, 1975). This system is interpreted to have been produced under considerably high temperature and pressure, because the (010) [100] slip system occurs under the highest temperature and pressure in comparison with other slip systems in light of the above experiments. Though no definite condition can be estimated for the formation of the slip system, extrapolation of the experimental results to the geologic strain rate (e.g. 10^{-13}/sec) indicates that the system would be produced at a condition higher than about 600°C under 15 kb.

2) Polygonal Olivine (Neoblastic-Recrystallized Olivine)

Polygonal olivine with straight boundaries, which shows a typical mosaic texture as shown in Text-fig. 11, is present in all ultramafic rocks of the Horoman massif. The polygonal olivine is clearly distinguished from the coarse deformed olivine on account of 1) equigranular and polygonal shape of grain, 2) lack of elongated and stretched grain, and 3) rare occurrence of kink bands. The grain size of polygonal olivine ranges from 0.05 to 2.00 mm in diameter and is conspicuously smaller than the porphyroclastic-primary grains. A marked difference in the grain size of polygonal olivine is found between the Lower Zone (0.05-1.00 mm) and the Upper Zone (0.40-2.00 mm).

In many "alpine-type" peridotites polygonal grains of olivine, which are described as mosaic grains or granulated matrix, have been commonly recognized as recrystallized products; e.g. Twin Sisters dunite (Ragan, 1963), Almklovdalen dunite (Lappin, 1967), Red Hill complex (Walcott, 1968), Piedmont Alps lherzolite (Nicolas et al., 1971) Burro Mountain peridotite (Loney et al., 1971), and Vulcan Peak peridotite (Himmerberg and Loney, 1973). The occurrence of the above recrystallized polygonal grains very resembles that of the polygonal olivine from the Horoman ultramafic rocks. In this connection, an experimental study on the recrystallization process of olivine was carried out by AvéLallemant and Carter (1970). This result shows that polygonal olivines were produced near the grain boundaries of the host grains at 1100°C and 13 kb. It was also observed that the intercrystalline recrystallization proceeded into the host grains. Accordingly, the Horoman polygonal olivine associated with coarse deformed olivine can be interpreted as a neoblast recrystallized from the coarse deformed olivine.

(3) Fine Olivine (Neoblastic-Granulated Olivine)

Fine olivine always shows irregular and anhedral form, and almost always lacks kink bands. The grain size is usually less than 0.4 mm. Most of the fine olivines show slightly elongated shape; the direction of elongation is nearly parallel to the foliation plane. The fine olivine occurs in monomineralic fine olivine seams formed by mylonitizatin and is found in all ultramafic rock types. A small amount of the fine

olivine is found in orthopyroxene + spinel seams of lherzolite and plagioclase + spinel seams of plagioclase lherzolite, which is distributed throughout the massif. A marked difference in occurrence of the fine olivine is noticed between the Lower and the Upper Zones. In the Lower Zone the monomineralic fine olivine seams are well developed. In the Upper Zone, however, the fine olivine seams are rather rare.

PYROXENE NEOBLASTS AND SYMPLECTITES

In some cases small-polygonal grains of pyroxenes are observed as neoblasts in dunite and lherzolite, and are rarely found in ultramafic parts of plagioclase lherzolite. The polygonal pyroxenes range from 0.01 mm to 0.5 mm in size and are commonly associated by large porphyroclastic ones.

It is probable that the pyroxene neoblasts were produced by intra- and inter-crystalline recrystallization from the porphyroclastic-primary grains of pyroxene.

Pyroxene-spinel symplectites are also found in lherzolite. The symplectites are common in the orthopyroxene + spinel seams of lherzolite. In rare cases orthopyroxene porphyroclast is replaced in part by pyroxene-spinel symplectite. The symplectite is classified into two types based on the mineral assemblages; one is orthopyroxene + clinopyroxene + spinel symplectite and the other is orthopyroxene + clinopyroxene + plagioclase + spinel symplectite. No symplectite has been found in the Upper Zone of the massif.

TEXTURAL DEVELOPMENT OF THE HOROMAN ULTRAMAFIC ROCKS

The following sequence of textural development after consolidation of the massif can be considered from the above descriptions on structure and texture of the Horoman ultramafic rocks (Niida, 1975).

The primary grains of porphyroclastic olivine were affected by plastic deformation, resulting in coarse deformed olivine with many kink bands of the (010) [100] slip system. Especially in the Lower Zone, elongated grains of the coarse deformed olivine were formed by translation gliding. Then or at the same time, recrystallization of olivine is considered to have occurred. Recystallization of pyroxenes also occurred at the same time and produced in part small neoblasts of pyroxenes and pyroxene-spinel symplectites.

Mineral chemistry

The chemical compositions of olivine, orthopyroxene, clinopyroxene, plagioclase, amphibole, and phlogopite were determined by quantitative electronprobe microanalysis. Polished thin sections of samples were coated with carbon film, about 500 Å in thickness. The measurements were performed with a JEOL:JXA-5A analyzer at the Geological Survey of Japan. Operating conditions were 15 kv in accelerating potential and 0.02-0.03μA in specimen current. The electron beam diameter was kept

Table 2 EPMA analyses and structural formulae for olivines from the Horoman ultramafic massif

No.	1	2	3	4	5	6	7	8	9	10	11	12
SiO_2	41.16	41.35	40.46	41.11	41.36	41.12	40.98	40.80	41.36	40.66	40.81	40.80
TiO_2	0.00	0.08	0.00	0.05	0.01	0.04	0.10	0.00	0.01	0.00	0.00	0.03
Al_2O_3	0.01	0.02	0.00	0.00	0.01	0.00	0.00	0.00	0.01	0.00	0.02	0.01
FeO*	7.32	7.92	7.90	7.97	8.12	8.26	8.40	8.60	8.46	8.90	8.92	9.03
MnO	0.12	0.15	0.17	0.12	0.12	0.16	0.13	0.19	0.12	0.14	0.16	0.13
MgO	50.52	51.39	51.39	50.96	50.68	50.60	50.28	50.91	50.34	50.40	50.03	50.06
CaO	0.04	0.00	0.02	0.02	0.01	0.02	0.01	0.02	0.02	0.02	0.02	0.02
Na_2O	0.03	0.00	0.01	0.02	0.02	0.00	0.01	0.01	0.00	0.02	0.00	0.01
Total	99.20	100.94	99.85	100.26	100.33	100.20	99.92	100.43	100.32	100.13	99.96	100.09
	Numbers of cations on the basis of 4 oxygens											
Si	1.004	0.995	0.986	0.996	1.001	0.998	0.998	0.990	1.003	0.992	0.996	0.995
Al	0.000	0.001	0.000	0.000	0.001	0.000	0.000	0.000	0.001	0.000	0.001	0.000
Ti	0.000	0.001	0.000	0.001	0.000	0.001	0.002	0.000	0.000	0.000	0.000	0.001
Fe**	0.149	0.159	0.161	0.162	0.165	0.168	0.171	0.175	0.172	0.181	0.182	0.184
Mn	0.002	0.003	0.002	0.003	0.003	0.004	0.003	0.002	0.003	0.003	0.003	0.003
Mg	1.837	1.843	1.866	1.840	1.829	1.830	1.826	1.842	1.819	1.832	1.820	1.820
Ca	0.001	0.000	0.001	0.001	0.000	0.001	0.000	0.001	0.001	0.000	0.000	0.001
Na	0.001	0.000	0.001	0.001	0.001	0.000	0.001	0.001	0.000	0.001	0.000	0.001
Total	2.994	3.002	3.016	3.004	3.000	3.002	3.001	3.011	2.999	3.009	3.002	3.005
M***	92.5	92.1	92.0	91.8	91.6	91.4	91.3	91.2	91.2	91.0	90.9	90.7
Sample	82808 D	82809 H.L.	72610 D	72611 D	73104 D	73101 D	70204 D	70602 L	72611 D	82402B L	82402B L	73016 L

*FeO = total iron expressed as FeO, **Fe = Fe^{+2}, ***M = 100 Mg/Mg+Fe+Mn

within 5-10 microns.

The following standard specimens were used; quartz for Si, rutile for Ti, corundum for Al, hematite for Fe, rhodonite for Mn, periclase for Mg, wollastonite for Ca, jadeite for Na, and adularia for K.

The data were corrected by the method of Sweatman and Long (1969) and Bence and Albee (1968). Calculation for correction and structural formula was carried out by using the computer programs developed by Okumura and Kawachi (1971), Kawachi (1971), Nakatsuka (1974), and Okumura and Soya (1975).

OLIVINE

Olivine is most dominant among the minerals in the Horoman ultramafic rocks. It constitutes more than 90% of dunite, 70-90% of harzburgite and lherzolite, and less than 80% of plagioclase lherzolite. Gabbro and pyroxenite contain a small amount of olivine. Textures in the ultramafic rocks are characterized by coexisting phases of porphyroclastic-primary olivine, recrystallized polygonal olivine, and mylonitized fine olivine.

The chemical composition and the structural formula of the olivines from the ultramafic and gabbroic rocks of the massif are given in Table 2. The forsterite content (100 Mg/Mg+Fe+Mn) in olivine from each rock type decreases from ultramafic to gabbroic rocks as shown in Text-fig. 12. The forsterite content of olivine ranges from 92.5 to 91.0 in dunite, 91.5 to 90.5 in lherzolite, 91.5 to 89.0 in plagioclase lherzolite,

Table 2 continued

No.	13	14	15	16	17	18	19	20	21	22	23	24
SiO_2	40.74	41.06	40.61	41.24	40.94	40.94	40.38	40.27	39.61	39.26	38.26	37.67
TiO_2	0.00	0.00	0.00	0.00	0.00	0.00	0.01	0.00	0.00	0.04	0.00	0.05
Al_2O_3	0.01	0.02	0.01	0.02	0.02	0.00	0.01	0.02	0.12	0.01	0.04	0.02
FeO*	9.08	9.34	9.48	9.55	9.60	10.07	10.76	10.72	15.35	16.71	26.28	30.32
MnO	0.17	0.14	0.17	0.12	0.17	0.13	0.13	0.15	0.23	0.39	0.44	0.56
MgO	49.65	49.47	49.28	49.41	49.17	49.15	49.25	48.57	44.71	43.65	36.27	30.81
CaO	0.01	0.02	0.15	0.01	0.03	0.02	0.01	0.01	0.08	0.02	0.01	0.03
Na_2O	0.00	0.01	0.02	0.02	0.00	0.02	0.03	0.00	0.00	0.04	0.04	0.01
Total	99.66	100.06	99.73	100.37	99.94	100.33	100.58	99.76	100.10	100.12	101.34	99.47
					Numbers of cations on the basis of 4 oxygens							
Si	0.998	1.003	0.997	1.004	1.002	1.000	0.989	0.994	0.995	0.993	1.000	0.998
Al	0.000	0.001	0.000	0.001	0.001	0.000	0.000	0.001	0.004	0.000	0.000	0.000
Ti	0.000	0.000	0.000	0.000	0.000	0.000	0.000	0.000	0.000	0.000	0.000	0.000
Fe**	0.186	0.191	0.195	0.195	0.197	0.206	0.220	0.221	0.322	0.353	0.575	0.704
Mn	0.004	0.003	0.004	0.003	0.004	0.003	0.003	0.003	0.005	0.008	0.010	0.014
Mg	1.813	1.800	1.803	1.793	1.794	1.790	1.797	1.787	1.674	1.646	1.413	1.284
Ca	0.000	0.001	0.004	0.001	0.001	0.001	0.000	0.000	0.002	0.000	0.000	0.001
Na	0.000	0.000	0.001	0.001	0.000	0.001	0.001	0.000	0.000	0.001	0.002	0.000
Total	3.001	3.000	3.004	2.998	2.999	3.001	3.010	3.007	3.002	3.001	3.001	3.001
M***	90.5	90.3	90.1	90.1	89.9	89.7	89.1	88.9	83.9	82.3	71.1	64.6
Sample	72601 L	72401 PL	73103 D	72607 PL	72402 PL	82201 PLII	82201 PLII	72906b Cpx L	82811b GB II	63003b GB	82308c GB	63014 GB

*FeO = total iron expressed as FeO, **Fe = Fe^{+2}, ***M = 100 Mg/Mg+Fe+Mn

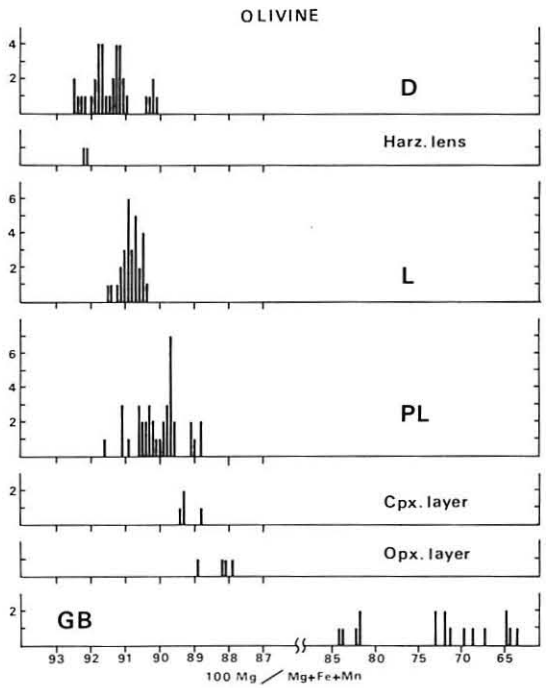

Text-fig. 12 Histogram showing the variation of 100 Mg/Mg+Fe+Mn ratio for olivines.

Table 3 EPMA analyses and structural formulae for orthopyroxenes from the Horoman massif

No.	1	2	3	4	5	6	7	8	9	10	11	12
SiO_2	57.14	56.59	56.66	57.03	56.59	57.36	57.25	56.11	56.80	55.86	55.47	55.39
TiO_2	0.12	0.02	0.00	0.08	0.08	0.07	0.08	0.00	0.06	0.00	0.06	0.09
Al_2O_3	2.27	2.12	1.94	1.19	2.91	1.93	1.93	3.31	3.03	4.16	2.71	3.78
FeO*	4.81	5.10	5.27	5.24	5.33	5.62	5.68	5.71	5.61	5.55	5.57	5.67
MnO	0.08	0.12	0.10	0.14	0.15	0.12	0.10	0.09	0.14	0.13	0.20	0.16
MgO	34.93	34.79	35.26	34.45	34.21	34.90	34.98	33.86	34.21	33.33	33.43	33.40
CaO	0.90	0.75	0.80	1.55	0.71	0.94	0.77	0.81	0.60	0.77	1.40	1.14
Na_2O	0.04	0.02	0.04	0.09	0.03	0.01	0.00	0.03	0.01	0.05	0.05	0.02
K_2O	0.00	0.00	0.00	0.00	0.00	0.01	0.00	0.00	0.01	0.00	0.00	0.00
Total	100.29	99.51	100.07	99.77	100.01	100.96	100.79	99.92	100.47	99.85	99.43	99.65
Numbers of cations on the basis of 6 oxygens												
Si	1.952	1.951	1.946	1.968	1.943	1.955	1.954	1.932	1.942	1.922	1.926	1.916
Al^{IV}	0.048	0.049	0.054	0.032	0.057	0.045	0.046	0.068	0.058	0.078	0.074	0.084
Al^{VI}	0.044	0.038	0.024	0.017	0.061	0.032	0.031	0.066	0.065	0.091	0.037	0.071
Ti	0.003	0.000	0.000	0.002	0.002	0.002	0.002	0.000	0.002	0.000	0.016	0.002
Fe**	0.137	0.147	0.152	0.151	0.153	0.160	0.162	0.164	0.160	0.160	0.162	0.164
Mn	0.002	0.003	0.003	0.004	0.005	0.003	0.003	0.003	0.004	0.004	0.006	0.005
Mg	1.778	1.788	1.805	1.772	1.750	1.772	1.779	1.737	1.743	1.709	1.730	1.721
Ca	0.033	0.028	0.030	0.057	0.026	0.034	0.028	0.030	0.022	0.029	0.053	0.042
Na	0.003	0.001	0.003	0.006	0.002	0.001	0.000	0.002	0.001	0.003	0.003	0.001
K	0.000	0.000	0.000	0.000	0.000	0.000	0.000	0.000	0.000	0.000	0.000	0.000
Total	4.000	4.005	4.017	4.009	3.999	4.005	4.005	4.002	3.997	3.996	4.006	4.006
M***	92.8	92.3	92.1	92.0	91.7	91.6	91.5	91.5	91.4	91.2	91.2	91.1
Fe**	7.0	7.5	7.6	7.6	7.9	8.1	8.2	8.5	8.3	8.4	8.3	8.5
Mg	91.3	91.1	90.8	89.5	90.7	90.1	90.4	89.9	90.5	90.0	89.0	89.3
Ca	1.7	1.4	1.6	2.9	1.4	1.8	1.4	1.6	1.2	1.6	2.7	2.2
Sample	82808 Opx L	72609 D	72703 D	82809 HL	73013 D	71002 D	71002 D	72707 L	72707 L	70203 L	73016 L	73016 L

*FeO = total iron expressed as FeO, **Fe = Fe^{+2}, ***M = 100 Mg/Mg+Fe+Mn

and 89.5 to 88.0 in pyroxenite. In the gabbroic layer (GB I), rapid increase in the Fe content of the olivine is observed from the margin (Fo_{85}) to the center (Fo_{64}), as shown in Text-fig. 12.

No difference in the ratio 100 Mg/Mg+Fe+Mn can be observed between porphyroclastic-primary olivine and polygonal-recrystallized olivine judging from the EPMA analyses. Additionally, no signs of compositional zoning are observed in large porphyroclasts of primary olivine.

Forsterite content of olivines from the Horoman ultramafic rocks shows a considerably wide range. Olivines from Horoman have a similar forsterite content to those from the Lizard lherzolite (Fo_{89-91}; Green, 1964) and from the Ronda lherzolite ($Fo_{87.8-91.7}$; Obata, 1980). The variations in those from the ultramafic tectonites such as from the Dun Mountain dunite ($Fo_{91.7}$; Challis, 1965), the Red Hill harzburgite ($Fo_{90.8}$; Challis, 1965), the Burro Mountain dunite and Harzburgite ($Fo_{91.0-92.7}$; Loney et al., 1971), which are considered to be depleted solid mantle fragments. A wide range of forsterite contents is also displayed by the magmatic series of dunite-wehrlite-clinopyroxenite. Olivines from the zones ultramafic complex have prominent variation in forsterite content; e.g. the Union Bay complex (Fo_{78-93}; Ruckmick and Noble, 1959) and the Duke Island complex (Fo_{78-91}; Irvine, 1974). Olivines in olivine-

Table 3 continued

No.	13	14	15	16	17	18	19	20	21	22	23	24
SiO_2	55.74	56.04	55.84	55.04	54.89	55.30	55.40	54.94	53.54	56.18	55.67	55.61
TiO_2	0.00	0.08	0.16	0.11	0.05	0.11	0.04	0.19	0.15	0.41	0.51	0.53
Al_2O_3	3.38	3.06	3.48	3.88	4.49	4.06	3.54	3.75	5.59	2.36	3.20	3.12
FeO*	5.90	6.12	6.05	6.30	6.48	6.58	6.76	6.86	6.68	7.56	7.61	7.73
MnO	0.11	0.14	0.19	0.12	0.17	0.14	0.18	0.18	0.21	0.12	0.14	0.12
MgO	33.73	33.77	33.44	33.26	33.03	33.04	32.55	32.97	31.30	32.74	32.49	31.90
CaO	0.97	0.83	0.79	0.73	0.88	0.75	1.04	0.48	1.86	0.92	1.42	1.73
Na_2O	0.04	0.01	0.03	0.05	0.05	0.03	0.03	0.04	0.08	0.04	0.05	0.08
K_2O	0.01	0.00	0.00	0.02	0.01	0.00	0.01	0.00	0.00	0.01	0.00	0.00
Total	99.88	100.05	99.98	99.51	100.05	100.01	99.55	99.41	99.41	100.34	101.09	100.82
	Numbers of cations on the basis of 6 oxygens											
Si	1.924	1.931	1.926	1.910	1.897	1.911	1.926	1.913	1.871	1.943	1.917	1.922
Al^{IV}	0.076	0.069	0.074	0.090	0.103	0.089	0.074	0.087	0.129	0.057	0.083	0.078
Al^{VI}	0.061	0.056	0.068	0.069	0.081	0.076	0.071	0.067	0.102	0.040	0.045	0.049
Ti	0.000	0.002	0.004	0.003	0.002	0.003	0.001	0.005	0.004	0.010	0.013	0.013
Fe**	0.160	0.177	0.175	0.183	0.187	0.190	0.197	0.200	0.195	0.218	0.219	0.223
Mn	0.003	0.004	0.006	0.004	0.005	0.004	0.005	0.005	0.006	0.003	0.004	0.003
Mg	1.735	1.735	1.718	1.720	1.701	1.704	1.686	1.710	1.676	1.688	1.667	1.643
Ca	0.036	0.031	0.029	0.027	0.033	0.028	0.039	0.017	0.070	0.034	0.052	0.064
Na	0.003	0.001	0.002	0.004	0.003	0.002	0.002	0.003	0.005	0.002	0.003	0.005
K	0.000	0.000	0.000	0.001	0.000	0.000	0.000	0.000	0.000	0.000	0.000	0.000
Total	4.009	4.006	4.002	4.011	4.012	4.007	4.001	4.007	4.012	3.995	4.003	4.000
M***	90.9	90.6	90.5	90.2	89.9	89.8	89.3	89.3	89.0	88.4	88.2	87.9
Fe**	8.8	9.1	9.1	9.5	9.7	9.9	10.3	10.4	10.3	11.3	11.3	11.6
Mg	89.4	89.3	89.4	89.1	88.6	88.7	87.7	88.7	86.0	87.0	86.0	85.1
Ca	1.8	1.6	1.5	1.4	1.7	1.4	2.0	0.9	3.7	1.7	2.7	3.3
Sample	72601 L	72606 PL	72607 PL	72401 PL	72902 PL	72402 PL	70807 Cpx L	72905 PL	70807 Cpx L	63006e Opx L	63006e Opx L	63006e Opx L

*FeO = total iron expressed as FeO, **Fe = Fe^{+2}, ***M = 100 Mg/Mg+Fe+Mn

clinopyroxene cumulates from some ophiolite complexes show a wide range of forsterite contents, e.g. the Green Hill complex (Fo_{79-90}; Mossman, 1973) and the Emigrant Gap (Fo_{74-85}; James, 1971).

ORTHOPYROXENE

Orthopyroxenes constitute about 5% of dunite, 10-20% of harzburgite and lherzolite, and 10-25% of plagioclase lherzolite. Large crystals of orthopyroxene are also contained in harzburgite lenses and orthopyroxenite layers. In the gabbroic parts of plagioclase lherzolite I and II, and gabbro I and II, orthopyroxene was not found, but only in the ultramafic parts. Generally, the porphyroclastic grains are anhedral and 1-8 mm in size. Many exsolution lamellae of Ca-rich pyroxene are observed in the host orthophyroxene porphyroclasts.

The chemical analyses and the structural formulae of orthopyroxenes from all the ultramafic rocks are given in Table 3. Only the host orthopyroxenes were analyzed, so that the values do not indicate the bulk compositions of orthopyroxene with lamellae. The ratio 100 Mg/Mg+Fe+Mn in the orthopyroxene decrease gradually from dunite to orthopyroxenite (Text-fig. 13). The (100 Mg/Mg+Fe+Mn) ratio in orthopyroxenes ranges from 92.5 to 91.0 in dunite, 91.5 to 90.0 in lherzolite, 90.5 to 89.0 in

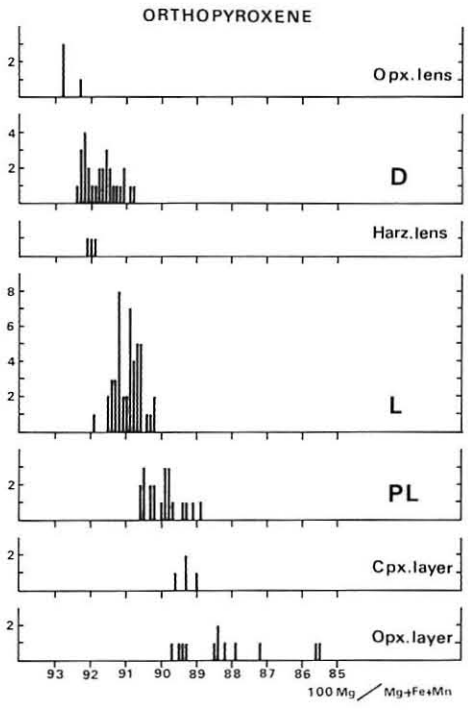

Text-fig. 13 Histogram showing the variation of 100 Mg/Mg+Fe+Mn ratio for orthopyroxenes.

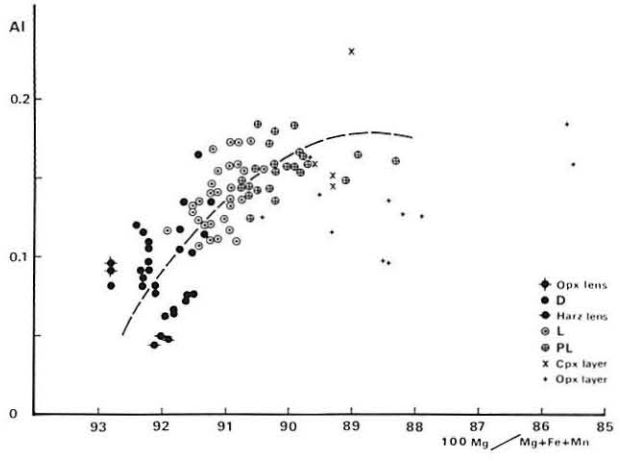

Text-fig. 14 Plot of total Al against 100 Mg/Mg+Fe+Mn ratio for orthopyroxenes.

plagioclase lherzolite, and 90.0 to 85.5 in clinopyroxentie and orthopyroxenite.

The CaO content of the Horoman orthopyroxenes ranges from 0.7 to 1.8 wt.% in primary grains. Very small polygons of recrystallized orthopyroxene, which are rarely found in and around host primary grains of the orthopyroxene from the Lower Zone of the massif, are considerably lower in CaO (less than 0.5 wt.%) than those of primary orthopyroxenes.

The Al_2O_3 content of the Horoman orthopyroxenes ranges from 1.2 to 5.6 wt.%. As shown in Text-fig. 14, the Al content increases from dunite to pyroxenite and also with increasing Fe contents. The Al_2O_3 content of orthopyroxenes ranges from 15.0 to 4.0 wt.% in dunite and dunitic harzburgite, 2.4 to 4.3, wt.% in lherzolite, 3.1 to 4.5 wt.% in plagioclase lherzolite, and 2.4 to 5.6 wt.% in pyroxenite. Discussions on pressure and temperature dependence of the solubility of Al_2O_3 in enstatitie have been made by many workers (Boyd and England, 1964; Anastasiou and Seifert, 1972; MacGregor, 1973; Arima et al., 1974; and Onuma and Arima, 1975). The Al_2O_3 content in orthopyroxenes from Horoman increases with Fe content. Petrological data obtained in the present study indicate that the residual liquid becomes rich in Fe with proceeding fractional crystallization, so that the minerals crystallized from this residual liquid would become also rich in Al content. It is also likely that the Horoman orthopyroxene becomes rich in Al with proceeding crystallization. Hence it is suggested that the Al_2O_3 content of the orthopyroxene is affected by chemical composition of the liquid from which the orthopyroxene crystallized out, rather than pressure and temperature.

Compositional zoning of Al_2O_3 and CaO contents is pronounced at the margin of orthopyroxene porphyroclasts. Cr_2O_3 content is slightly zoned at the margin. These three contents decrease outward. At the contact with chromian spinels, the zoning pattern of orthopyroxene is disturbed. Compositional plateaus having the highest and uniform content in Al_2O_3, CaO, and Cr_2O_3 can be recognized at the core of orthopyroxene grains. Fe/Mg ratio, however, is nearly uniform throughout the grains. As mentioned in the later chapter, the zoning pattern is considered to have been formed by diffusion process during deformation and recrystallization under different pysicochemical conditions. The highest contents in Al_2O_3, CaO, and Cr_2O_3 at the central plateau of orthopyroxenes probably indicate a primary composition.

CLINOPYROXENE

Clinopyroxene occurs in all rock types of the massif, but in the dunite aggregations of fine grained clinopyroxene occur only sporadically. The lherzolite and the plagioclase lherzolite contain 5-20% clinopyroxene, which is anhedral and ranges from 1 to 5 mm in grain size. Many exsolution lamellae of orthopyroxene, parallel to (100) of host clinopyroxene, are easily observed under the microscope (Yamaguchi and Tomita, 1970).

The chemical analyses and the structural formulae of the clinopyroxenes are given in Table 4. The main crystallization course of the Horoman clinopyroxene is $Ca_{46}Mg_{50.5}Fe_{3.5} \rightarrow Ca_{49}Mg_{46.5}Fe_{4.5} \rightarrow Ca_{50}Mg_{43.5}Fe_{6.5} \rightarrow Ca_{38}Mg_{39}Fe_{23}$ is shown in Text-fig. 15. Variation of the compositions is in harmony with change of rock types, from diopside in the ultramafic rock to salite ~ calcic augite in the gabbroic rocks. In the series of ultramafic rocks a gradual increase in the Fe and Ca content with decrease in the Mg content is observed in clinopyroxenes from dunite to plagioclase lherzolite through lherzolite. In gabbro the Ca and Mg contents decrease while the Fe content

Table 4 EPMA analyses and structural formulae for clinopyroxenes from the Horoman ultramafic massif

No.	1	2	3	4	5	6	7	8	9	10	11	12
SiO_2	54.31	54.39	54.20	53.86	53.61	54.33	52.99	54.32	51.70	52.00	51.20	51.51
TiO_2	0.00	0.12	0.06	0.10	0.12	0.04	0.03	0.07	0.63	0.39	0.55	0.78
Al_2O_3	2.43	1.88	1.95	2.50	3.28	3.31	4.28	3.13	5.57	4.74	5.72	5.33
FeO*	1.96	1.92	1.98	2.17	2.21	2.22	2.33	2.31	2.58	2.80	3.01	3.09
MnO	0.06	0.07	0.11	0.10	0.08	0.12	0.03	0.09	0.10	0.09	0.00	0.12
MgO	17.36	17.49	17.53	17.09	16.83	17.14	16.93	17.33	15.46	16.05	15.17	15.10
CaO	22.05	24.07	24.41	23.45	23.38	22.22	22.03	21.68	22.66	22.41	22.76	22.95
Na_2O	0.82	0.27	0.23	0.62	0.60	0.77	0.79	0.75	0.76	0.76	0.83	0.72
K_2O	0.01	—	—	0.00	0.00	0.00	0.00	0.01	0.00	0.01	0.00	0.00
Total	99.00	100.20	100.47	99.89	100.11	100.15	99.41	99.69	99.46	99.25	99.24	99.60
					Numbers of cations on the basis of 6 oxygens							
Si	1.977	1.964	1.956	1.954	1.940	1.956	1.925	1.963	1.886	1.902	1.877	1.883
Al^{IV}	0.023	0.036	0.044	0.046	0.060	0.044	0.075	0.037	0.114	0.098	0.123	0.117
Al^{VI}	0.081	0.044	0.039	0.061	0.080	0.097	0.108	0.097	0.125	0.106	0.134	0.113
Ti	0.000	0.003	0.002	0.003	0.003	0.001	0.001	0.002	0.017	0.011	0.015	0.021
Fe**	0.060	0.058	0.060	0.066	0.067	0.067	0.071	0.070	0.079	0.086	0.092	0.094
Mn	0.001	0.002	0.003	0.003	0.002	0.004	0.001	0.003	0.003	0.003	0.000	0.003
Mg	0.942	0.942	0.943	0.924	0.908	0.920	0.917	0.933	0.841	0.875	0.829	0.822
Ca	0.860	0.931	0.944	0.912	0.907	0.857	0.858	0.839	0.886	0.878	0.894	0.899
Na	0.058	0.019	0.016	0.043	0.042	0.054	0.056	0.052	0.054	0.054	0.059	0.051
K	0.000	—	—	0.000	0.000	0.000	0.000	0.000	0.000	0.001	0.000	0.000
Total	4.002	3.999	4.007	4.012	4.009	4.000	4.012	3.996	4.005	4.014	4.013	4.003
Fe**	3.3	2.9	3.1	3.5	3.5	3.6	3.8	3.8	4.3	4.7	5.1	5.3
Mg	50.6	48.6	48.4	48.6	48.3	49.9	49.7	50.7	46.6	47.6	45.6	45.3
Ca	46.1	48.5	48.5	47.9	48.2	46.5	46.5	45.5	49.1	47.7	49.3	49.5
Sample	72703 D	71002 D	71002 D	72704 L	72611 D	72601 L	72707 L	72603 L	72607 PL	72606 PL	72402 PL	629-1 PL

*FeO = total iron expressed as FeO, **Fe = Fe^{+2}

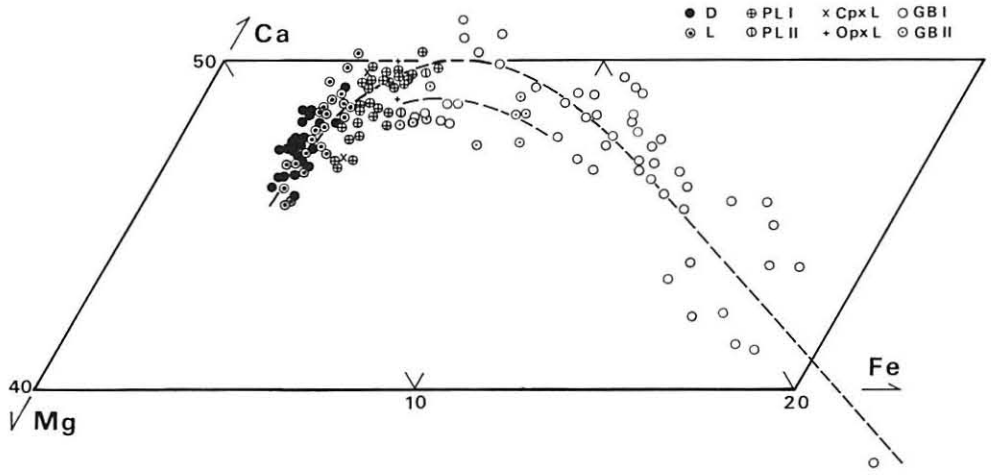

Text-fig. 15 Variation in chemical composition of clinopyroxenes from the Horoman massif.

Table 4 continued

No.	13	14	15	16	17	18	19	20	21	22	23	24
SiO_2	51.64	51.18	52.31	50.49	51.14	50.75	48.10	49.57	49.39	50.71	50.47	49.99
TiO_2	1.13	1.10	0.11	0.90	1.01	0.23	2.16	1.28	1.45	0.62	0.78	0.75
Al_2O_3	4.11	4.75	3.83	7.33	5.13	6.35	7.07	5.64	5.42	3.85	3.81	4.10
FeO*	3.47	3.36	3.60	3.55	4.08	5.87	6.71	7.69	8.26	9.87	10.72	13.68
MnO	0.09	0.09	0.14	0.11	0.14	0.12	0.20	0.18	0.24	0.25	0.34	0.31
MgO	16.11	15.34	15.57	14.91	15.10	14.13	12.91	13.33	13.09	12.69	13.90	12.86
CaO	23.49	23.61	23.71	22.00	22.99	23.01	22.30	21.19	21.09	21.24	19.52	17.32
Na_2O	0.57	0.70	0.51	0.68	0.47	0.52	0.83	0.79	0.78	0.59	0.47	0.59
K_2O	0.01	0.01	—	0.00	0.00	0.00	0.01	0.01	0.01	0.01	0.00	0.00
Total	100.57	100.14	99.78	99.97	100.06	100.98	100.29	99.68	99.73	99.83	100.01	99.60
					Numbers of cations on the basis of 6 oxygens							
Si	1.879	1.871	1.912	1.838	1.871	1.853	1.785	1.847	1.846	1.903	1.890	1.894
Al^{IV}	0.121	0.129	0.088	0.162	0.129	0.147	0.215	0.152	0.154	0.097	0.110	0.106
Al^{VI}	0.055	0.075	0.077	0.153	0.092	0.127	0.094	0.095	0.083	0.073	0.058	0.077
Ti	0.031	0.030	0.003	0.025	0.028	0.006	0.060	0.035	0.040	0.018	0.022	0.021
Fe**	0.104	0.103	0.110	0.108	0.125	0.179	0.208	0.239	0.258	0.310	0.336	0.433
Mn	0.003	0.003	0.004	0.003	0.004	0.004	0.005	0.005	0.007	0.008	0.011	0.010
Mg	0.874	0.836	0.848	0.809	0.824	0.769	0.714	0.740	0.729	0.710	0.776	0.736
Ca	0.916	0.925	0.928	0.858	0.901	0.901	0.887	0.846	0.844	0.854	0.783	0.703
Na	0.040	0.050	0.034	0.048	0.033	0.037	0.050	0.057	0.056	0.043	0.034	0.044
K	0.000	0.000	—	0.000	0.000	0.000	0.000	0.000	0.000	0.001	0.000	0.000
Total	4.023	4.022	4.004	4.004	4.007	4.023	4.025	4.016	4.017	4.017	4.020	4.014
Fe**	5.5	5.5	5.8	6.1	6.8	9.7	11.5	13.1	14.1	16.5	17.7	23.3
Mg	46.2	44.9	45.0	45.6	44.5	41.6	39.5	40.6	39.8	37.9	41.0	39.0
Ca	48.3	49.6	49.2	48.3	48.7	48.7	49.0	46.3	46.1	45.6	41.3	37.7
Sample	82201 PLII	82201 PLII	82811a GBII	82206 GBI	82202a GBI	82811b GBII	63006b GBI	63015 GBI	63015 GBI	00421 GBI	63014 GBI	00421 GBI

*FeO = total iron expressed as FeO, **Fe = Fe^{+2}

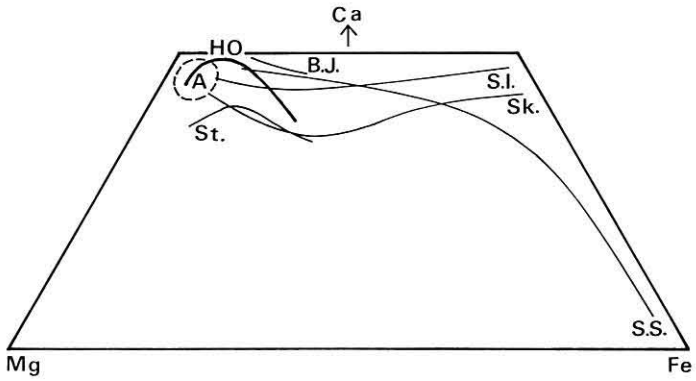

Text-fig. 16 Di-Hd-En-Fs diagram showing crystallization courses of clinopyroxens.
HO: Horoman (this work). B.J.: Black Jack sill (Wilkinson, 1957) S.S.: Shonkin Sag laccolith (Nash and Wilkinson, 1970). S.I.: Shiant Isles sill (Gibb, 1973). Sk.: Skaergaard intrusion (Wager and Brown, 1967). St.: Stillwater complex (Hess, 1960). A: "alpine-type" peridotites (Green, 1964; Challis, 1965; Loney et al., 1971; Himmerberg and Loney, 1973; Mossman, 1973).

rapidly increases. Clinopyroxenes from gabbro I plot in the wollastonite-rich field beyond the tie line of diopside — hedenbergite, indicating that these clinopyroxenes are very high in Ca content as shown in Text-fig. 15. Clinopyroxene from gabbro II, however, is somewhat lower in Ca content and the crystallization course is also shown in Text-fig. 15. The crystallization course of the clinopyroxene observed in the Horoman ultramafic massif is clearly different from that of the "alpine-type" peridotites (Green, 1964; Challis, 1965; Loney et al., 1971; Himmerberg and Loney, 1973), of the tholeiitic layered instrusions (Hess, 1960; Wager and Brown, 1967), and

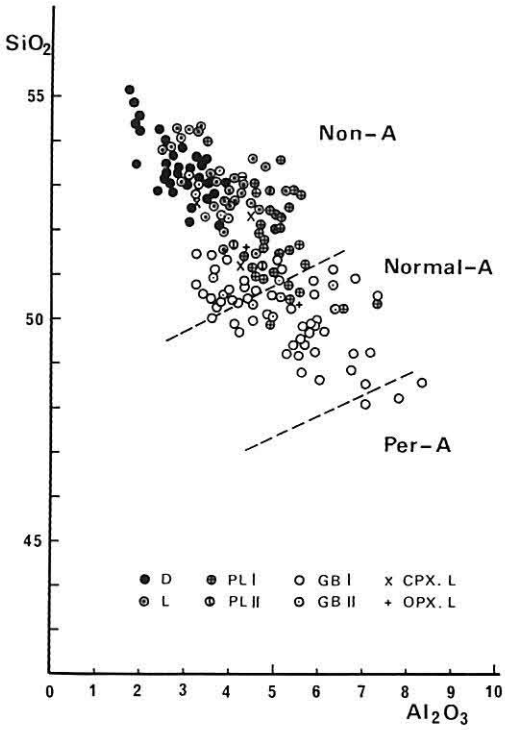

Text-fig. 17 Relation between SiO_2 and Al_2O_3 in the Horoman clinopyroxenes.

of the basic alkaline rocks (Murray, 1954; Wilkinson, 1957; Nash and Wilkinson, 1970; Gibb, 1973), as shown in Text-fig. 16. However, most analyses of clinopyroxene from the Horoman ultramafic rock series, dunite, lherzolite, and plagioclase lherzolite, fall into the region of clinopyroxenes from "alpine-type" peridotite. The Horoman clinopyroxenes from the margin of gabbro I layer have similar compositions to those from the earlier phase clinophyroxenes of peralkaline rocks such as Black Jack sill (Wilkinson, 1957) and Shokin Sag laccolith (Nash and Wilkinson, 1970). Moreover, compositions of clinopyroxenes from the Horoman gabbro II are also similar to those from mildly alkaline rocks such as Shiant Isles sill (Gibb, 1973).

Clinopyroxenes from the "zoned-type" complexes of Union Bay (Ruckmick and Noble, 1959) and of Duke Island (Irvine, 1974) have similar crystallization course to

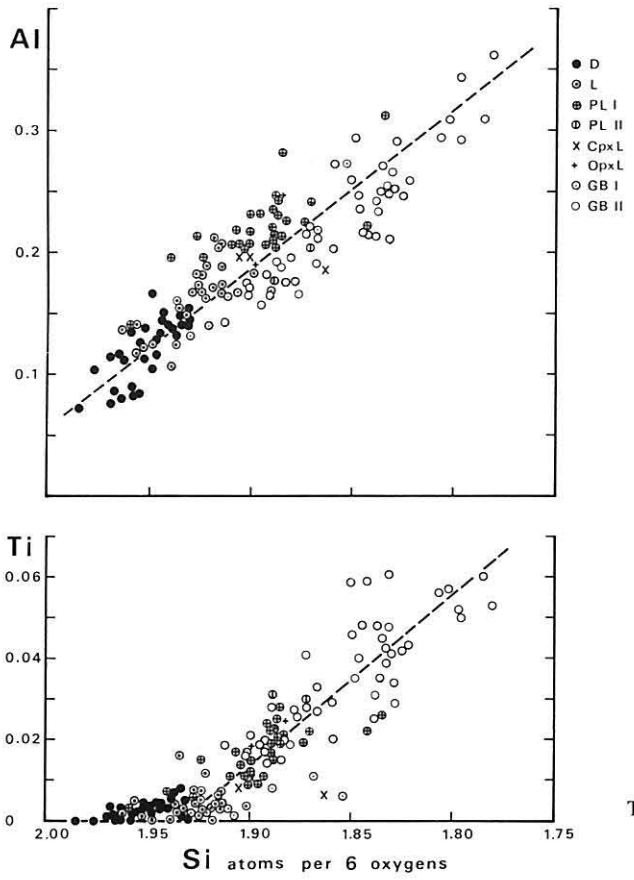

Text-fig. 18 Variations in total Al and Ti with Si atoms per 6 oxygens of the Horoman clinopyroxenes.

the Horoman clinopyroxene, although these pyroxenes are lower in Ca content.

The SiO_2-Al_2O_3 relation of the Horoman clinopyroxenes is shown in Text-fig. 17. The clinopyroxene from the ultramafic rocks is higher in SiO_2 and lower in Al_2O_3, whereas that from the gabbroic rocks is higher in Al_2O_3 and lower in SiO_2. Text-fig. 17 clearly indicates a gradual change of the SiO_2 and Al_2O_3 contents in the Horoman clinopyroxene. The Al_2O_3 content of clinopyroxene gradually increases with change of rock types from ultramafic rocks (1.6-3.3 wt.% in dunite, 2.5-5.0 wt.% in lherzolite, 4.1-7.3 wt.% in plagioclase lherzolite) to the gabbroic rocks (3.2-8.4 wt.% in GB I, and 3.8-6.4 wt.% in GB II).

Kushiro (1960) and LeBas (1962) suggested that clinopyroxene compositions depend on the degree of alkalinity of their parentage, and that the SiO_2-Al_2O_3 relations could be used to indicate the nature of the original magma. However, Gibb (1973) studied the zoned clinopyroxenes in the alkaline rocks of the Shiant Isles sill and showed that the plots of the clinopyroxene analyses from the same parent magma are scat-

tered all over the non-alkaline, alkaline, and per-alkaline fields in the SiO_2-Al_2O_3 diagram given by LeBas (1962). Therefore, it is not reliable to use this diagram to presume the parentage of magma, but it can be used to estimate the nature of the liquid from which the pyroxene in question is crystallizing out. Consequently, the SiO_2-Al_2O_3 relation of the Horoman clinopyroxenes seems to be affected essentially by the chemical composition of the residual liquid changing its composition with proceeding fractionation.

Plotting total Al and Ti against Si atoms in the Horoman clinopyroxenes (Text-fig. 18) reveals that the Al and Ti content increases linearly with decrease of the Si content. These values are lower in the clinopyroxenes from the dunite and higher in those from the gabbros. All of the total Al plots lie in the Al-rich side from the Si + Al = 2 line, suggesting that Si deficiency in Z group is completely supplemented by Al. The straight lines in Text-fig. 18 show Al:Si = 1.3:1 and Ti:Si = 0.5:1 respectively, indicating the coupled substitution of $R^{2+} + 2\,Si \rightleftharpoons Ti^{4+} + 2\,Al$ suggested by the several investigators (Ross et al., 1970; Barberi et al., 1971; Gibb, 1973). The relationship between Ti and Al^{IV} is $2\,Ti = Al^{IV}$ and between Al^{IV} and Al^{VI} is $Al^{VI} = Al^{IV}$. When Al^{IV} increases, Al^{VI} and Ti also increase. Consideration on these relations leads to the following substitution.

$$Mg + 2\,Si \rightleftharpoons Ti + 2\,Al^{IV}$$
$$Mg\,Si \rightleftharpoons Al^{VI}\,Al^{IV}$$

Consequently, Ca-tschermak's molecule ($CaAl_2SiO_6$) and titanpyroxene molecule ($CaTiAl_2O_6$) increase gradually with the change of rock types from dunite to gabbros. In the gabbroic rocks, the titanpyroxene molecule is more abundant than Ca-tschermak's molecule, judging from the Al^{VI}-Al^{IV} diagram. It is more likely that the content of Al and Ti in the Horoman clinopyroxenes is affected by the change of the

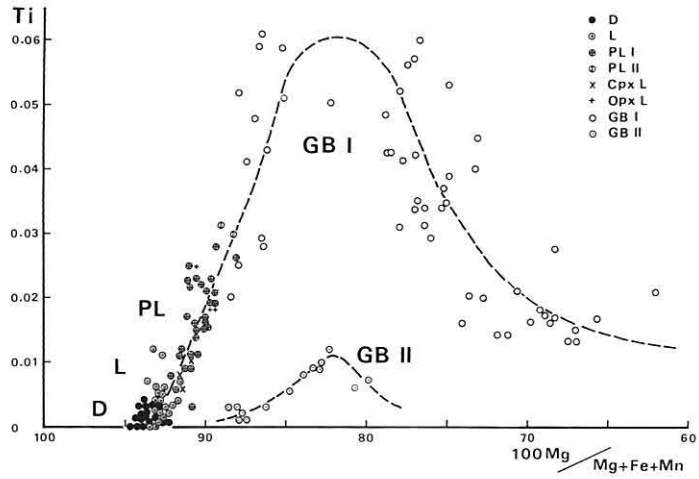

Text-fig. 19 Plots of Ti vs. 100 Mg/Mg+Fe+Mn ratio showing variation in Ti content of the Horoman clinopyroxenes with fractional crystallization.

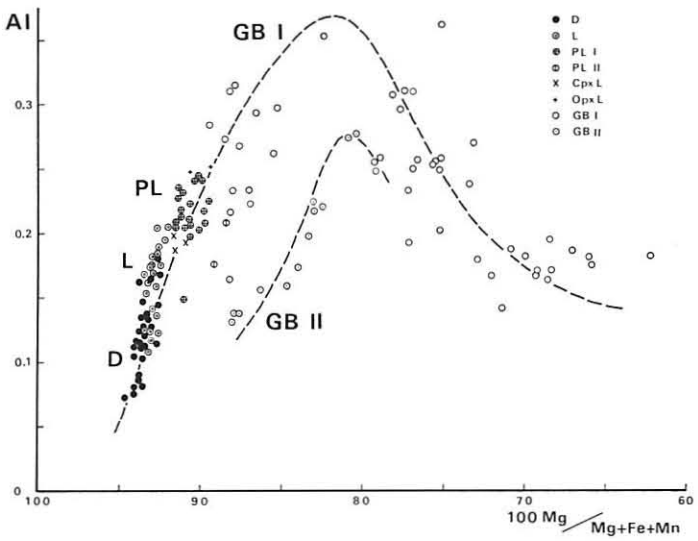

Text-fig. 20 Plots of total Al vs. 100 Mg/Mg+Fe+Mn ratio showing variation in Al content of the Horoman clinopyroxenes with fractional crystallization.

composition of residual liquid.

The Na_2O content of the Horoman clinopyroxenes ranges from 0.2 to 1.4 wt.%: 0.2 to 0.6 wt.% Na_2O in clinopyroxenes from dunite, 0.5 to 0.9 wt.% in lherzolite, 0.6 to 1.4 wt.% in plagioclase lherzolite, and 0.5 to 1.0 wt.% in gabbro. Hence, there is no major difference in the Na_2O content of clinopyroxenes from each rock type. Therefore, the solubility of jadeite molecule may be rather low and constant.

Clinopyroxenes from alkaline rocks have higher Al and Ti content than those from the other rock types as generally known. On the basis of thermodynamic consideration Verhoogen (1962) suggested that the Al and Ti contents of clinopyroxenes are essentially a reflection of the SiO_2 concentration and oxygen partial pressure in magma. Carmichael et al. (1970) and Bargeri et al. (1971) also indicated that the composition of clinopyroxene is strongly influenced by SiO_2 activity. Several works on the solubility of TiO_2 content in pyroxene have been carried out (e.g., Yagi and Onuma, 1967). Maximum content of TiO_2 in the Horoman clinopyroxenes is 2.4 wt.%.

The variation pattern of Ti content in the Horoman clinopyroxenes against the 100 Mg/Mg+Fe+Mn ratio (M value), which is a scale of fractionation, is shown in Text-fig. 19. The Ti content of the clinopyroxene successively increases with change of rock types from dunite to gabbro I through lherzolite and plagioclase lherzolite. The solubility of TiO_2 attains a maximum at about $M = 82$ which occurs at the margin of gabbroic layers. With further fractionation the Ti content decreases. A similar Ti variation is observed in gabbro II (Text-fig. 19), although the Ti content of the clinopyroxene is very small.

The total Al content of the clinopyroxene shows a similar variation trend to that of Ti content, and the maximum solubility is also reached at about M = 82 as shown in Text-fig. 20.

Similar trends are observed in Ti-rich pyroxenes in akaline rocks from several localities; e.g. Morotu alkaline rocks (Yagi, 1953) and Garbh Eilean sill of Shiant Isles (Murray, 1954; Gibb, 1973). From the experimental study on the joint $CaMgSi_2O_6$-$CaTiAl_2O_6$, Yagi and Onuma (1967) suggested that the TiO_2 content increases at the earlier stage and gradually decreases in the middle to later stage. The variation trend of TiO_2 in the pyroxene observed in the present study agrees with their suggestion. Different mineral assemblages are observed before and after the maximum solubility of Ti. Before the maximum solubility, Ti-rich dioside coexists with kaersutites and Ti-pargasites in the margin of gabbroic layer, whereas after that the diopside becomes Ti-poor and coexists with ilmenite and titano- and titaniferous magnetites instead of kaersutite and Ti-pargasite. However, in some cases the kaersutite coexists with ilmenite. The pyroxene, therefore, changes in composition with proceeding fractional crystallization as follows.: Ti-poor diopside → salite → calcic augite. After reaching the maximum Ti-solubility, the Ti-rich diopside develops many lamellae of kaersutite or Ti-pargasite, suggesting that the solubility of TiO_2 in the clinopyroxene decreases.

KAERSUTITE, Ti-PARGASITE AND PARGASITE

Ti-pargasites were found in gabbroic seams of plagioclase lherzolite I and II and in layers of gabbro I. Usually the Ti-pargasite occurs in small grains less than 0.5 mm and

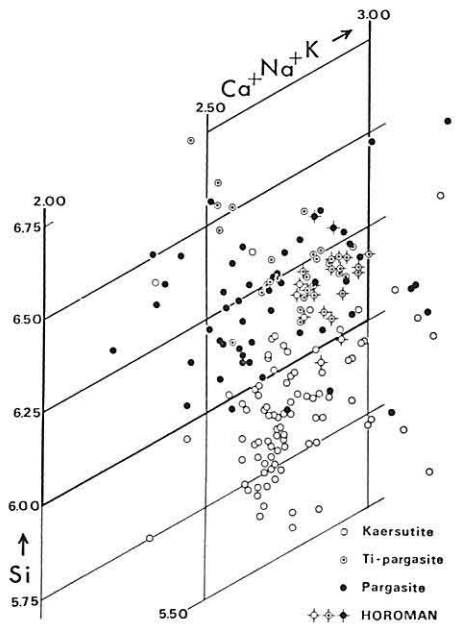

Text-fig. 21 Si vs. Ca + Na + K relation of kaersutites, Ti-pargasites and pargasite from the world (Niida, 1977), symbols with cross are those from the Horoman gabbroic series.

Table 5 EPMA analyses and structural formulae for kaersutites, Ti-pargasites and pargasites from the Horoman ultramafic massif

	1	2	3	4	5	6	7	8	9	10	11	12
SiO_2	42.60	43.82	43.55	43.54	43.45	43.26	43.11	42.05	41.58	41.45	44.50	44.03
TiO_2	3.38	3.94	4.08	3.65	4.44	5.34	5.02	5.52	3.61	4.05	0.85	0.85
Al_2O_3	13.82	12.91	13.04	12.76	12.21	12.47	11.68	11.91	12.60	13.09	13.12	13.45
FeO*	4.27	4.55	4.77	4.99	5.52	5.82	6.39	6.65	10.20	10.82	6.12	6.33
MnO	0.09	0.06	0.10	0.08	0.08	0.09	0.07	0.17	0.14	0.21	0.13	0.06
MgO	17.21	16.70	16.32	16.86	16.28	15.71	16.09	15.63	13.74	13.25	17.20	17.88
CaO	12.29	12.85	12.37	12.34	12.06	12.25	11.84	11.81	12.21	11.87	12.29	12.21
Na_2O	3.18	3.26	3.68	3.40	3.35	3.21	3.42	3.34	3.43	3.59	3.40	3.63
K_2O	0.22	0.33	0.13	0.26	0.07	0.08	0.06	0.09	0.07	0.08	0.02	0.04
Total	97.06	98.42	98.04	97.88	97.46	98.23	97.68	97.17	97.58	98.41	97.63	97.48
	Numbers of cations on the basis of 23 oxygens											
Si	6.109	6.210	6.198	6.213	6.233	6.170	6.203	6.105	6.113	6.058	6.363	6.320
Al^{IV}	1.891	1.790	1.802	1.787	1.767	1.830	1.797	1.895	1.887	1.942	1.637	1.680
Al^{VI}	0.445	0.367	0.386	0.359	0.299	0.267	0.184	0.144	0.296	0.314	0.576	0.596
Ti	0.364	0.420	0.437	0.391	0.479	0.573	0.543	0.602	0.399	0.445	0.092	0.091
Fe**	0.512	0.539	0.567	0.596	0.662	0.694	0.769	0.807	1.255	1.323	0.732	0.760
Mn	0.011	0.008	0.012	0.010	0.010	0.011	0.009	0.020	0.017	0.026	0.016	0.007
Mg	3.677	3.528	3.462	3.585	3.480	3.340	3.450	3.381	3.011	2.887	3.666	3.610
Ca	1.888	1.951	1.886	1.887	1.854	1.872	1.826	1.838	1.924	1.859	1.884	1.878
Na	0.885	0.896	1.016	0.942	0.932	0.888	0.954	0.941	0.978	1.017	0.943	1.011
K	0.039	0.060	0.024	0.048	0.012	0.015	0.011	0.017	0.013	0.015	0.004	0.007
Total	15.821	15.769	15.790	15.818	15.728	15.660	15.746	15.750	15.893	15.886	15.913	15.960
M***	87.5	86.6	85.7	85.5	83.8	82.6	81.6	80.4	70.3	68.2	83.1	82.5
Sample	72902 PLI	82201 PLII	70803 PLI	82201 PLII	82202a GBI	82202a GBI	82202a GBI	82202a GBI	82308c GBI	82308c GBI	82811a GBII	82811a GBII

*Fe = total iron expressed as FeO, **Fe = Fe^{+2}, ***M = 100 Mg/Mg+Fe+Mn

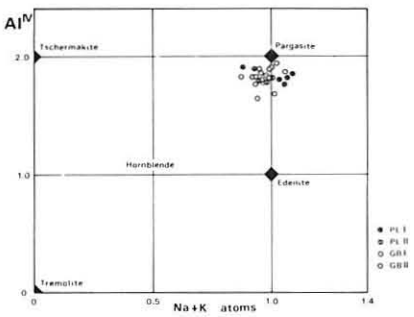

Text-fig. 22 Al^{IV} vs. Na+K plots of kaersutite, Ti-pargasite, and pargasite from the Horoman gabbroic series.

is associated with clinopyroxenes (Text-fig. 21). The Ti-pargasite shows strong pleochroism from almost colorless to pale brown or reddish brown in thin section, and $2V_Z = 84° - 90°$. The Ti-pargasite in the Horoman gabbro has been described as a pale brown hornblende by Igi (1953) and Niida (1974). Small amounts of Ti-poor pargasite were also found in the layers of gabbro II. These pargasites are 1.0 mm in maximum grain size, and show weak pleochroism from colorless to pale green and $2V_Z = 83° - 92°$.

The chemical compositions and the structural formulae of the Ti-rich and Ti-poor pargasites from gabbro I and II of the Horoman massif are given in Table 5. The Na+K content in these paragasites is 0.85-1.10, and the Al atoms in tetrahedral sites are 1.70-1.95 as shown in Text-fig. 22. The Horoman Ti-pargasite contains up to

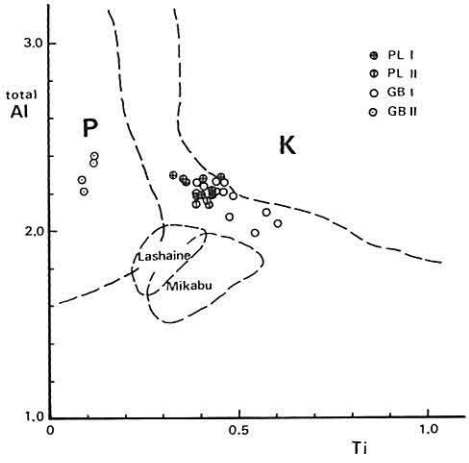

Text-fig. 23 Total Al vs. Ti relation of the Horoman kaersutite, Ti-pargasite, and pargasite. P and K show pargasite and kaersutite fields defined by the data from the world (Inomata and Tazaki, 1974). Ti-pargasites of alkali pyroxenite xenoliths from the Lashine Volcano (Dawson and Smith, 1973) and wehrlite from the Mikabu zone (Inomata and Tazaki, 1974) are also shown.

5.5 wt.% TiO_2. According to Aoki and Matsumoto (1959), kaersutite contains more than 5.0 wt.% TiO_2, and Leake (1968) called amphibole containing more than 0.5 Ti atomic numbers kaersutite. Taking these definitions into account, some of the Horoman Ti-pargasite correspond to kaersutite.

Plots of total Al against Ti in the Horoman kaersutites, Ti-pargasites, and

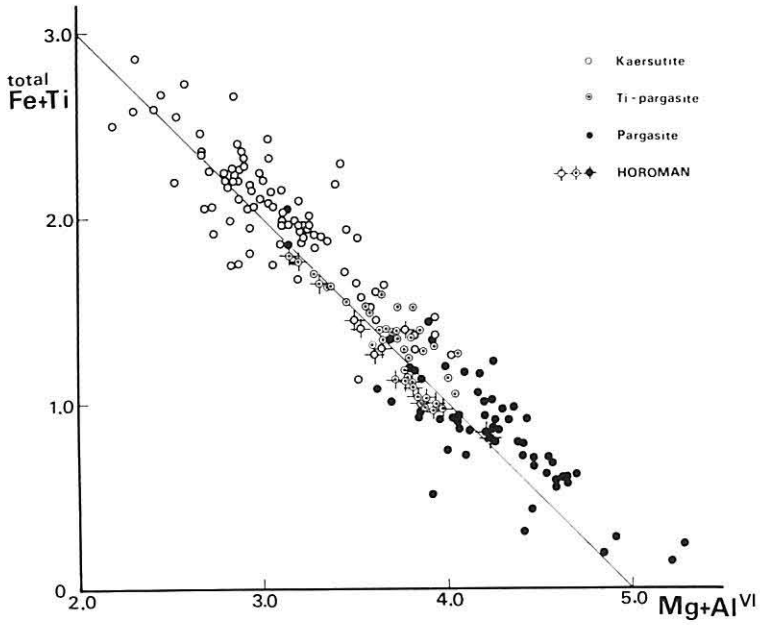

Text-fig. 24 Total Fe + Ti vs. Mg + Al^{VI} relation of kaersutite, Ti-pargasite, and pargasite from the world (Niida, 1977); marks with cross represent those from the Horoman gabbroic series.

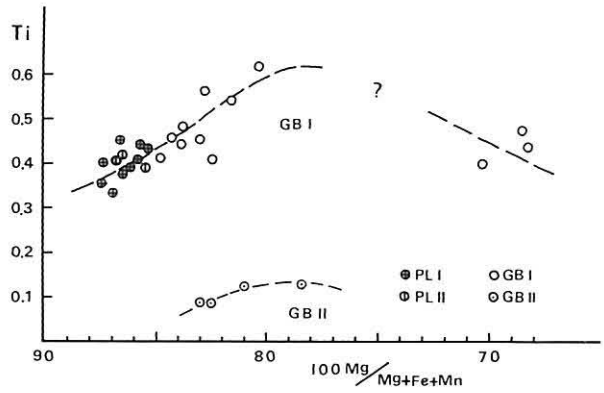

Text-fig. 25 Plot of Ti vs. 100 Mg/Mg+Fe+Mn ratio showing variation in Ti content of the Horoman kaersutites, Ti-pargasites, and pargasites with fractional crystallization.

pargasites are given in Text-fig. 23. The relations between kaersutite and pargasite have been discussed by Wilkinson (1961), Wilshire et al. (1971), and Wilshire and Trask (1971). Wilkinson (1961) suggested that kaersutite corresponds to titaniferous pargasite with the substitution of Mg by Fe^{2+}, and gave the general formula of $(Na, K, Ca)_{2-3}(Mg_3, Fe^{2+})TiAl^{IV}{}_2Si_6O_{23}(OH)$. Natural occurrence of kaersutite produced by the reaction between pargasite and basanite magma has been reported by Wilshire et al. (1971). These studies show the intimate relationship between kaersutite and pargasite.

Recently, Ti-pargasites were found in alkalic pyroxenite xenoliths from Lashine Volcnao (Dawson and Smith, 1973) and in wehrlites from the Mikabu zone in Japan (Inomata and Tazaki, 1974; Tazaki and Inomata, 1974).

Mutual relations among the chemical compositions of kaersutite, Ti-pargasite, and pargasite in the world and shown in Text-fig. 24. It is evident from this figure that the substitution of $Fe+Ti \rightleftharpoons Mg+Al^{VI}$ in the octachedral site as well as $Si \rightleftharpoons Al^{IV}$ in the tetrahedral site takes place in these minerals. The Horoman Ti-rich and Ti-poor pargasites are continuously distributed from the pargasite field to the kaersutite through the Ti-pargasite field (Text-fig. 24). Therefore, some of the Horoman Ti-pargasite have a similar character to kaersutites. Petrogenesis of the kaersutite-bearing rocks was discussed in detail by Yagi (1953) and Aoki and Matsumoto (1959). It is considered that the Horoman kaersutite and Ti-pargasite characterize the gabbro I as an alkaline rocks.

Plots of the Ti content of the kaersutite, Ti-pargasite, and pargasite against the ratio 100 Mg/Mg+Fe+Mn (M value) show a trend similar to that of the clinopyroxenes (Text-fig. 25). The Ti content gradually increases toward the maximum solubility at $M=78$, then decreases. The variation trend indicates that composition of the Horoman amphiboles was controlled mainly by the chemical composition of magma.

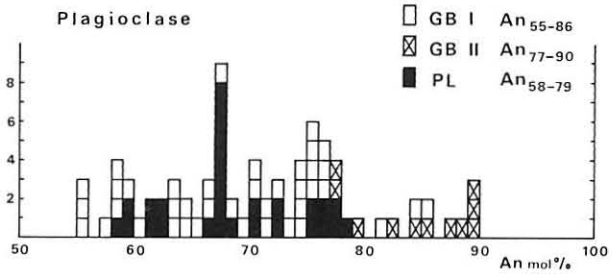

Text-fig. 26 Histogram of An mol. % of plagioclase from the Horoman gabbroic series.

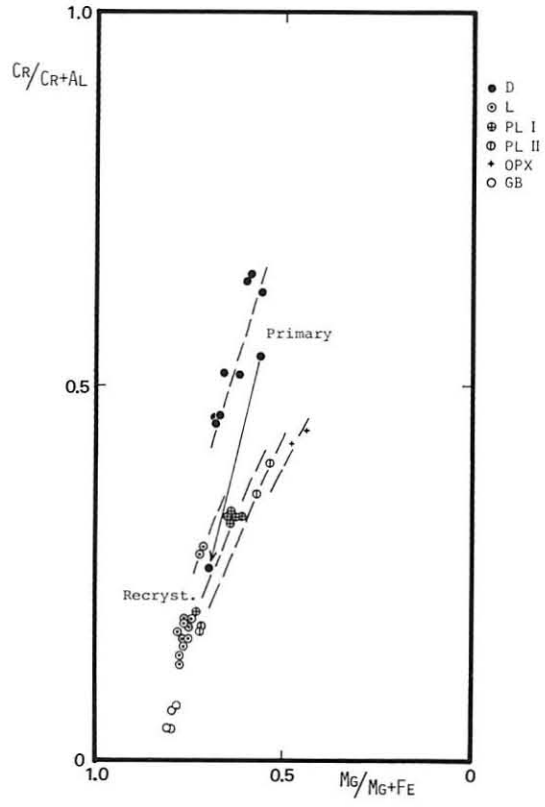

Text-fig. 27 Cr/Cr+Al vs. Mg/Mg+Fe plots of spinels from the Horoman massif.

PLAGIOCLASE

Plagioclases occur in gabbroic seams of plagioclase lherzolite I and II, and gabbro I and II. The grain shape is usually anhedral.

The chemical analyses given in Table 6 show a wide range from An_{55} to An_{90} (mol. %). Such a wide composition range is also observed in each rock type (Text-fig. 26). Plagioclases from the plagioclase lherzolite range from An_{58} to An_{79} (mol. %), and those from the gabbro I ranges from An_{55} to An_{86}. Plagioclases from the gabbro II are more calcic, An_{77} to An_{90}.

Table 6 EPMA analyses and structural formulae for plagioclases from the Horoman ultramafic massif

	1	2	3	4	5	6	7	8	9	10	11	12
SiO_2	46.84	46.67	46.94	47.70	48.99	48.51	49.01	50.45	50.69	50.44	53.28	53.50
TiO_2	0.00	0.11	0.05	0.02	0.00	0.03	0.06	0.03	0.00	0.00	0.04	0.18
Al_2O_3	34.38	33.84	33.70	33.27	32.68	32.53	31.91	31.15	31.02	31.32	29.31	29.13
FeO	0.20	0.20	0.15	0.18	0.00	0.07	0.24	0.08	0.08	0.09	0.03	0.08
MnO	0.00	0.02	0.03	0.00	0.12	0.03	0.04	0.00	0.00	0.00	0.03	0.00
MgO	0.02	0.00	0.00	0.02	0.00	0.00	0.01	0.06	0.03	0.04	0.02	0.05
CaO	18.16	17.54	17.34	16.87	16.21	15.99	15.32	14.72	14.44	14.40	12.50	12.40
Na_2O	1.23	1.45	1.74	2.04	2.58	2.72	2.88	3.14	3.38	3.60	4.68	4.84
K_2O	0.00	0.00	0.02	0.01	0.01	0.02	0.01	0.03	0.04	0.04	0.08	0.01
Total	100.84	99.83	99.97	100.11	100.59	99.89	99.48	99.66	99.68	99.93	99.97	100.19
Numbers of cations on the basis of 32 oxygens												
Si	8.549	8.597	8.633	8.747	8.920	8.898	9.061	9.224	9.264	9.204	9.660	9.677
Al	7.396	7.348	7.307	7.192	7.014	7.035	6.871	6.716	6.684	6.740	6.264	6.212
Ti	0.000	0.015	0.008	0.003	0.000	0.000	0.000	0.004	0.000	0.000	0.008	0.025
Fe**	0.031	0.031	0.023	0.028	0.000	0.011	0.037	0.012	0.012	0.012	0.004	0.012
Mn	0.000	0.003	0.005	0.000	0.018	0.005	0.006	0.000	0.000	0.000	0.004	0.000
Mg	0.005	0.000	0.000	0.004	0.000	0.000	0.002	0.016	0.008	0.012	0.008	0.015
Ca	3.552	3.462	3.418	3.316	3.162	3.142	2.998	2.884	2.828	2.816	2.428	2.402
Na	0.435	0.518	0.620	0.726	0.910	0.968	1.020	1.112	1.196	1.272	1.648	1.699
K	0.000	0.000	0.006	0.002	0.002	0.004	0.003	0.008	0.008	0.008	0.020	0.002
Total	19.970	19.974	20.020	20.018	20.029	20.063	20.006	19.976	20.000	20.064	20.044	20.044
An	89.1	87.0	84.6	82.0	77.2	75.6	74.6	72.1	70.2	68.9	59.4	58.6
Ab	10.9	13.0	15.3	17.9	22.2	23.3	25.3	27.8	29.6	30.9	40.1	41.3
Or	0.0	0.0	0.1	0.1	0.6	1.1	0.1	0.1	0.2	0.2	0.5	0.1
Sample	82811b GBII	82811b GBII	82206 GBI	82811a GBII	629014 PL	82402b PL	82308c GBI	72607 PL	72905 PL	72912 PL	72606 PL	82202a GBI

*Fe = total iron expressed as FeO, **Fe = Fe^{+2}

Table 7 EPMA analyses and structural formulae for phlogopites from the Horoman ultramafic massif

		1	2	3	4
SiO_2		40.64	39.01	39.83	40.29
TiO_2		6.52	6.45	5.67	6.44
Al_2O_3		16.35	15.64	16.31	16.34
Fe_2O_3*		3.54	3.46	3.61	3.64
MnO		0.01	0.03	0.02	0.01
MgO		21.83	21.01	21.21	20.21
CaO		0.01	0.02	0.01	0.00
Na_2O		1.79	1.95	1.63	1.85
K_2O		7.72	8.21	7.96	8.53
Total		98.41	95.78	96.25	97.31
Formulae on basis of O = 22					
Z	Si	5.48	5.44	5.50	5.52
	Al (IV)	2.52	2.56	2.50	2.48
Y	Al (VI)	0.08	0.01	0.15	0.16
	Fe**	0.36	0.36	0.38	0.38
	Ti	0.66	0.68	0.59	0.66
	Mn	0.00	0.00	0.00	0.00
	Mg	4.38	4.37	4.36	4.12
X	Ca	0.00	0.00	0.00	0.00
	Na	0.47	0.53	0.44	0.49
	K	1.33	1.46	1.40	1.49
Z		8.00	8.00	8.00	8.00
Y		5.48	5.42	5.48	5.32
X		1.80	1.99	1.84	1.98
Mg/Mg+Fe**		0.924	0.924	0.920	0.916

*Fe_2O_3 = total iron expressed as Fe_2O_3
**Fe = Fe^{+3}

SPINEL

Primary grains of spinel are found in dunite, plagioclase lherzolite I and II, gabbro I, and rarely in lherzolite. Many small grains of recrystallized spinel are aggregated with orthopyroxenes in the fine grained seams of lherzolite. Furthermore, recrystallized spinels, occur as pyroxene-spinel symplectites.

According to the chemical analyses by Bamba (1953), Nagasaki (1966) and the EPMA analyses in this work (Table 7), spinels are highly variable in composition. As shown in Text-fig. 27, reddish brown spinels in dunite are Cr-rich with Cr/Cr+Al ratios from 0.45 to 0.65. Brown spinels in gabbroic seams of plagioclase lherzolite have a considerably wide range of the Cr/Cr+Al ratio from 0.15 to 0.40 and the Mg/Mg+Fe ratio from 0.54 to 0.74. Green spinels from the margin of GB I are characteristically rich in Al and Mg.

PHLOGOPITE

A phlogopite vein was found in lherzolite of the Horoman massif (Niida, 1975). The phlogopite is 2.0 mm in maximum grain size, and is accompanied by small crystals of brown spinel. The phlogopite shows strong pleochroism from almost colorless to pale brown or reddish brown in thin sections, and often exhibits wavy extinciton. $2V_X$ is 5°-9°, with a concentration between 7° and 8°.

The chemical analyses are given in Table 7. The Mg and Ti contents of the Horoman phlogopite are very high. The occurrence and the chemical compositon suggest that the Horoman phlogopite was crystallized out at the latest stage of fractional crystallization.

Petrogenesis

PRIMARY CRYSTALLIZATION

The characteristics of chemical composition of the primary minerals and their occurrences indicate that the genesis of the Horoman ultramafic massif can be explained by a successive fractional crystallization that produced a series of rocks from dunite to gabbro. Mineral variation with the crystallization of the Horoman ultramafic massif is summarized in Text-fig. 28.

From the facts mentioned above it is considered that the main sequence of the fractional crystallization resulted in the following rock series: dunite → lherzolite → plagioclase lherzolite → gabbro I (margin to center). The texture of dunite indicates that olivine, orhtopyroxene, and spinel crystallized at the earliest stage of crystallization. The olivine formed at the earliest stage is rich in MgO ($Fo_{92.5}$). The MgO content of olivine gradually decreases with proceeding crystallization, and Fe-rich olivine (Fo_{64}) crystallized at the final stage. The orthopyroxene also crystallized at the earliest stage. The enstatite content is high ($En_{93.0}$) in the earliest stage of the crystallization

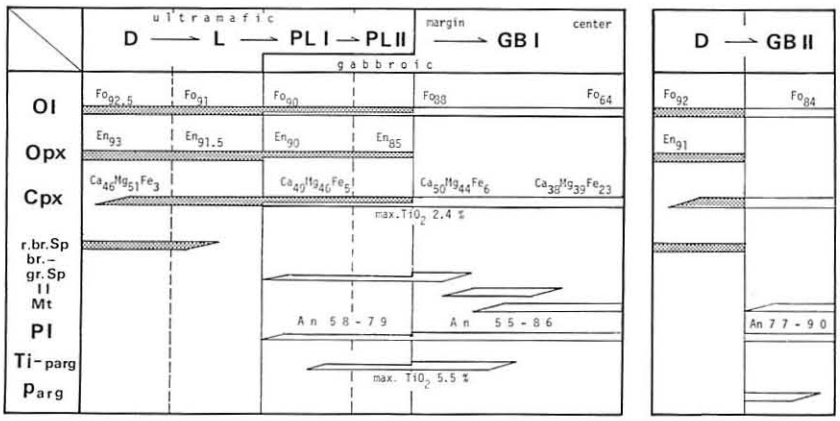

Text-fig. 28 Mineral variation with crystallization sequence in the Horoman massif. Stippled bars: primary minerals in the ultramafic series, open bars: those in the gabbro series.

gradually decreasing to $En_{85.5}$ in the later stage. However, no orthopyroxene is found in the gabbroic rocks. The clinopyroxene probably crystallized slightly later than the olivine and orthopyroxene, and continuously changed in composition from diopside in ultramafic rocks to calcic augite in gabbros. The content of Ca, Al, and Ti in the clinopyroxene shows a similar trend. The clinopyroxenes having the maximum solubility of these elements are observed in the specimens from the marginal parts of the gabbro I layer. The chromian spinel crystallized as a primary mineral. On the other hand, spinel, ilmenite, titano-and titaniferous magnetite and magnetite crystallized out one after another in the later stage. Ti-rich minerals occurring in the marginal parts of the gabbro I, are titaniferous diopside, kaersutite, Ti-pargasite, and ilmenite.

Another crystallization sequence, dunite → gabbro II, is also found in the Horoman ultramafic massif. This sequence is locally observed in the Upper Zone of the massif. In this sequence olivines are rich in MgO content and have a limited range in composition (Fo_{92} to Fo_{84}). The clinopyroxenes also have a narrow range ($Ca_{46}Mg_{51}Fe_3$ to $Ca_{48}Mg_{46}Fe_6$). The variation in Ca, Al, and Ti contents of clinopyroxenes is markedly different from that of the main crystallization sequence. It is noticed that the Ti-poor pargasite and calcic plagioclase are associated with the olivine and the clinopyroxene in this sequence.

It seems that all the gabbroic parts were formed by the crystallization of residual liquid at the middle to later stage. The fine-grained gabbroic seams in plagioclase lherzolite I were probably formed by the crystallization of interstitital liquid, and those of the plagioclase lherzolite II, which is a transitional type between the plagioclase lherzolite I and thin bands of the gabbro I, also resulted from a more abundant interstitial liquid. The thin bands and thick layers (approximately 30 m in maximum thickness) of gabbro I which are common type in the Upper Zone, were crystallized from the residual liquid at the later or the latest stage of the crystallization. It is considered from the chemical composition of rocks and constituent minerals that the gabbro II was

formed by crystallization of the MgO-rich residual liquid enclosed in the solid phase of dunite and crystallized at the earlier stage.

The following observations suggest that the residual liquid of the Horoman massif gradually changed from non-alkaline to alkaline with proceeding fractional crystallization.

1) Ti-rich minerals such as titaniferous diopside to salite, kaersutite, Ti-pargasite, and ilmenite crystallized from the residual liquid are characteristically present in the marginal rocks of gabbro I. Orthopyroxene did not crystallize from the residual liquid. Olivine crystals in gabbro have no reaction rim. The olivine continued to crystallize until the latest stage. These are characteristic in alkaline rocks.

2) The Ca, Al, and Ti contents of the Horoman clinopyroxenes continuously increase with proceeding fractional crystallization. The Ca-tschermak's molecule and titan-pyroxene molecule contents of the clinopyroxenes are lower in dunite, and become higher in gabbro. Furthermore, some clinopyroxenes from the gabbro I plot on the wollastonite side of the diopside-hedenbergite join. This phenomenon has never been reported in clinopyroxenes from non-alkaline rocks.

3) In the SiO_2—Al_2O_3 diagram clinopyroxenes from dunite and lherzolite plot in the non-alkaline field, whereas many clinopyroxenes from gabbro plot in the alkaline field. This indicates that the residual liquid becomes alkaline with proceeding fractional crystallization.

Field evidence of partial melting has been discussed on some "alpine-type" periodotites; the Almklovdalen peridotite by Carswell (1968), the Ronda peridotite by Dickey (1970) and Dickey et al. (1977), the Lanzo peridotite by Boudier and Nicolas (1977), and the Josephine peridotite by Dick (1977). Boudier and Nicolas (1977) reported feldspathic veins and dykes formed by partial fusion of peridotite and dunite was thought to be residual. In the case of olivine websterite, which is regarded as a trapped partial melt from the Josephine peridotite (Dick, 1977), the minerals in the residual peridotites show a systematic variation in composition from pyroxene-rich to more refractory pyroxene-poor harzburgite.

The most important problem is understanding how the gabbro in the Horoman layered sequence formed. The residual magma model for the Horoman gabbros, explained above, has several advantages over a partial melting model.

The following evidence negates the partial melting model.

1) The gabbroic layers (GB I) generally occur in plagioclase lherzolites which represent the more Fe-rich rocks in the Horoman ultramafic rock series. In the Upper Zone the gabbro I is often interlayered with Fe-rich dunite. In both cases, the ratio Fe/Mg+Fe in ferromagnesian minerals continuously increases toward gabbros throughout the ultramafic rock series. Hence, it is more likely that the variation trend of Fe/Mg+Fe is a result of fractional crystallization.

2) The Horoman layered sequence is characterized by the diverse rock series, dunite → lherzolite → plagioclase lherzolite → gabbro, which shows a systematic variation in composition. The mineralogy also shows wide systematic ranges in chemical compositions (Text-fig. 28). As might be expected, fractional crystallization produces diverse

lithologies and wide variations in chemical composition of silicate minerals, while partial melting is expected to leave a solid residue of nearly uniform composition (Presnall, 1969).

CRYPTIC LAYERING AND ITS ORIGIN

The term cryptic layering, which has been commonly used in the layered intrusins (e.g. Hess, 1969; Wager and Brown, 1967; Wager, 1968), means the inconspicuous and gradual change in mineral compositions toward upsection. It is one of the most important phenomena used in explaining the genesis of layered sequences. The cryptic variation of minerals in the Horoman layered sequence is summarized in Text-fig. 29.

The cryptic variation of olivine, orthopyroxene, and plagioclase, observed in the Lower Zone of the Horoman ultramafic massif is in harmony with the lithological change in layering. Forsterite content of olivine shows a successive variation from lower to upper compositional layers. The cryptic layering of olivine shows a "symmetrical and wavy" pattern, in which the maximum Fo content is found at the center of the dunite layers, and the minimum at the center of the plagioclase lherzolite. The cryptic variation in enstatite content of orthopyroxene is consistent with the Fo content of the coexisting olivine. These features of cryptic layering disagree with Nagasaki's results (Nagasaki, 1962, 1966).

It is noted that the minimum values of Fo content of olivine and En content of orthopyroxene occur at the centers of the plagioclase lherzolite layers and that the values slightly decrease upward in the massif. This is an important tendency that Fe content of the minerals gradually increases from the bottom to the top of the massif.

Mol. % An of plagioclase in the plagioclase lherzolite from the Lower Zone decreases toward the center of the layers (Text-fig. 29).

In the Upper Zone of the massif, however, the cryptic layering is characterized by a rapid and successive variation in accordance with the lithological changes in the layering. Text-fig. 30 shows the cryptic layering in the gabbro I layer (1 m in thickness) in the Upper Zone. The composition of olivines varies continuously from Fo_{89} at the margin of the layer to Fo_{64} at the center. Variation of the 100 Mg/Mg+Fe+Mn ratio of clinopyroxenes is similar to that of olivines. The TiO_2 content of clinopyroxenes also varies from 2.4 wt.% at the margin to 0.5 wt.% at the center.

Origin of the Horoman ultramafic layered sequence is not explained well by the concept of crystal sinking used in the Skaergaard, Stillwater, and other layered complexes. Several concepts for origin of the layering in the "alpine-type" peridotites have been proposed. However, none of them adequately explains the origin of well-developed layered structure observed in the Horoman massif. Therefore, the present writer proposes a new mechanism for the formation of layered sequences in the "alpine-type" peridotite (Text-fig. 31).

At the later stage of crystallization the Horoman massif probably reached a stage when it possessed an alkaline residual liquid within solid phases of ultramafic ones. Before the alkaline liquid was formed, the crystallization of the Horoman massif pass-

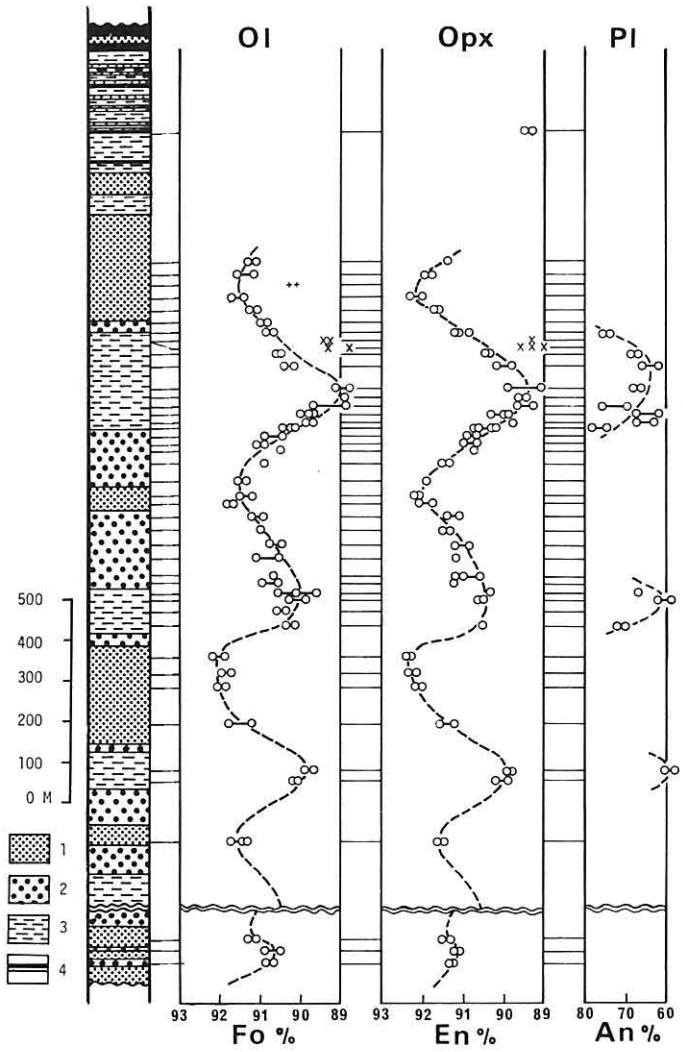

Text-fig. 29 Cryptic variation in Fo content of olivine, En content of orthopyroxene, and An content of plagioclase, in the columnar section along the Horoman River. 1: dunite, 2: lherzolite, 3: plagioclase lherzolite, 4: gabbro.

ed through a non-alkaline crystal mush stage (Stage I). The crystallization in the Lower Zone proceeded slightly more than that in the Upper Zone as inferred from the consistent increase in Fe content of the ferromagnesian silicates upward in the massif. Subsequent to the non-alkaline crystal mush stage, the crystallization proceeded to a stage at which the ultramafic solid phases crystallized out and the residual liquid became alkaline in chemical composition (Stage II).

At this stage, the Lower Zone, composed mainly of the ultramafic rocks, is considered to have almost solidified, except for very small pockets of residual liquid at

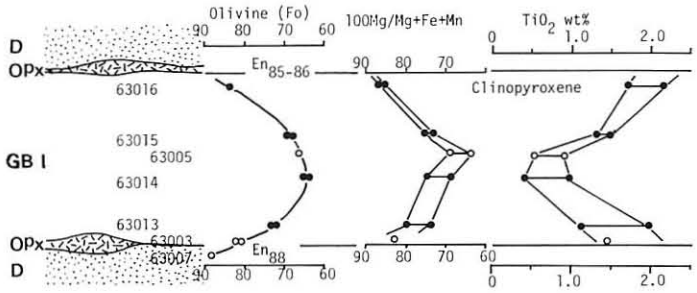

Text-fig. 30 A cryptic variation in gabbro I layer (1 m in thickness) from the Upper Zone of the Horoman massif.

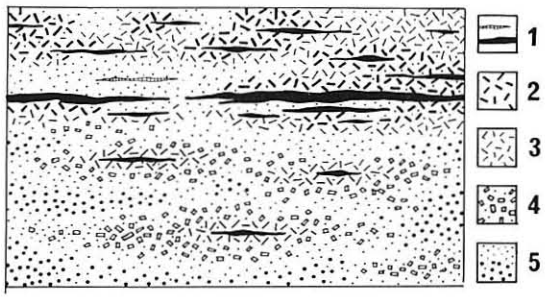

Text-fig. 31 Schematic diagram illustrating the residual magma stage of crystallization of the Horoman massif in the upper mantle. 1. Residual liquids of the gabbro I (black) and gabbro II (shaded) trapped in ultramafic solid phases. 2. Interstitial liquids trapped in ultramafic solid phases of plagioclase lherzolite II. 3. Interstitial liquids trapped in ultramafic solid phases of plagioclase lherzolite I. 4. Lherzolites already solidified. 5. Dunites composed of Mg-rich olivines (large dots) and Fe-rich olivines (small dots).

several parts. It is thought that the ultramafic solid phase around the residual liquid was plagioclase lherzolite in which some interstitial liquid still remained. A zonal arrangement of inner plagioclase lherzolite with the interstitial liquid outward to lherzolite, and dunite, was probably formed from the pocket of the residual liquid. A tendency of Fe-enrichment in the liquid also occurred with crystallization since Mg-rich minerals crystallized at the earlier stage are found in the dunite and Fe-rich minerals in the plagioclase lherzolite.

It must be noted that the residual liquid concentrated mainly in the Upper Zone of the massif at the same time. The plagioclase lherzolite I and II with interstitial liquid is also thought to have crystallized around the pockets of the residual liquid that formed the gabbro I. The residual liquid producing gabbro II was included locally in dunite of the Upper Zone.

While the residual liquid still remained, intrusion of the whole massif probably took place (Stage III). This movement resulted in formation of the layering. The symmetrical pattern of the cryptic layering, as well as phase layering, was formed by internal sliding of the massif. In the ultramafic rocks, which were already solidified, deformation and recrystallization took place especially in the Lower Zone, and the strongly strained grains of olivine and pyroxene were formed near the lowest parts of the massif. On the other hand, the crystallization proceeded in the residual liquid. The interstitial liquid crystallized into the fine grained gabbroic seams in the plagioclase lher-

zolite I and II. Additionally, the residual liquid crystallized to form thin bands and thick layers of gabbro I. Both lineations with igneous and tectonic characters are considered to have formed parallel to the direction of the movement at this stage.

Subsequent to the complete consolidation, the Horoman massif intruded in the solid state toward the present level along the deep-seated thrust fault zone (Stage IV). Many seams composed of the monomineralic fine olivine were formed near the bottom of the massif during the uplift. At the final stage of the emplacement the Horoman massif was affected by fracturing and weak serpentinization near the surface. Aggregations of small grains of talc and tremolite were formed along the fractures before the emplacement at the present position.

RECRYSTALLIZATION AND RE-EQUILIBRATION

As mentioned in the chapters of petrography and mineralogy, the Horoman ultramafic rocks are strongly modified by deep-seated deformation and recrystallization. The following modifications by recrystallization are observed:

1) Primary olivine → recrystallized olivine
2) Aluminous orthopyroxene → orthopyroxene + clinopyroxene + spinel
3) Aluminous orthopyroxene → orthopyroxene + clinopyroxene + spinel + plagioclase
4) Aluminous orthopyroxene → orthopyroxene + plagioclase + spinel
5) Aluminous orthopyroxene + spinel → orthopyroxene + aluminous spinel

Pyroxene-spinel symplectites formed by breakdowns 2), 3) and 4) are rarely observed in the aluminous orthopyroxenes. Primary chromian spinels can not be found in lherzolite. The spinels and aluminous orthopyroxenes are expected to be transformed into orthopyroxene + spinel seams, which are commonly observed in the lherzolite, by reaction 5).

As shown in Text-fig. 32, two different trends in compositional variation can be traced; one is a primary crystallization trend showing Fe-enrichment in orthopyroxene and the other is a recrystallization and re-equilibration trend showing Ca-depletion caused by diffusion between solid phases. The highest value in the Ca/Ca+Mg+Fe of orthopyroxenes reaches approximately 3.0 at the earliest stage of the crystallization. The value increases and eventually reaches about 3.3 at the later stage. The Ca-depletion trend is recognized as a compositional zoning of Ca/Ca+Mg+Fe in primary orthopyroxene porphyroclasts, as shown by the tie-lines from the core (C) to the margin (M) of primary grains in Text-fig. 32. As might be expected, recrystallized grains (R) have very low values of Ca/Ca+Mg+Fe ranging from 0.5 to 1.5. The Horoman clinopyroxenes are also zoned at the periphery of the primary grains.

Recognition of primary compositions of pyroxenes has been carried out by compositional mapping (Obata, 1980). The primary composition may be regarded as a high and uniform compositional plateau in the primary orthopyroxenes. As for the Horoman orthopyroxenes the primary composition can be obtained by step-scanning EPMA analyses (Text-fig. 33). The variation patterns of Al_2O_3 and CaO contents form the highest, flat, uniform compositional plateaus at the core of the primary grains of

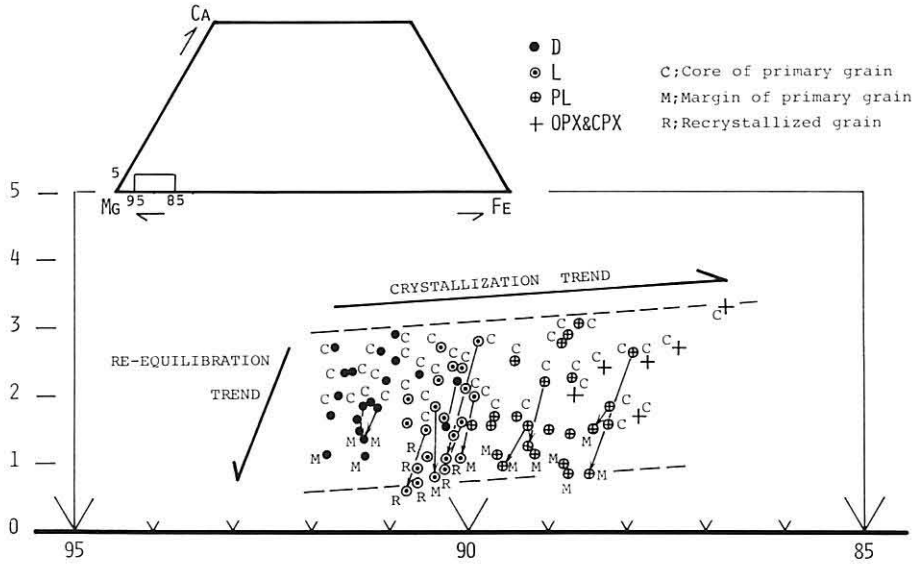

Text-fig. 32 Crystallization and re-equilibration trends of orthopyroxenes from the Horoman ultramafic series.

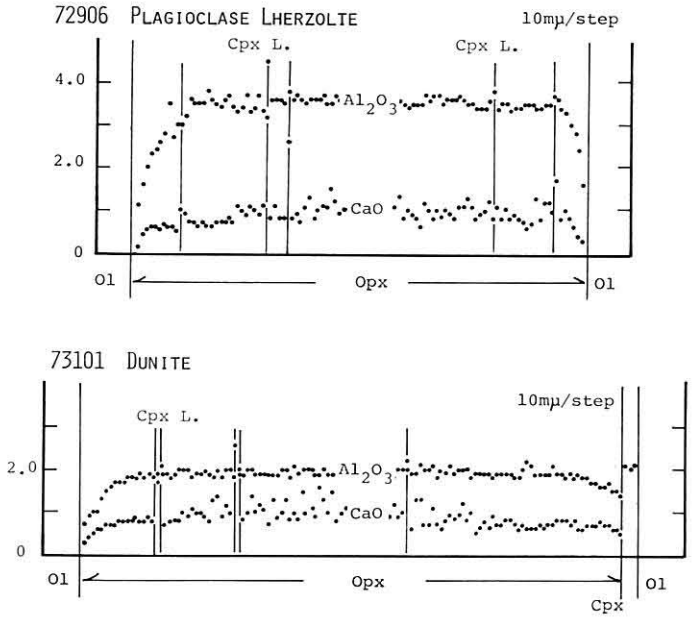

Text-fig. 33 Zoning patterns obtained by step-scanning EPMA analyses, showing variations in Al_2O_3 and CaO of orthopyroxene porphyroclasts from plagioclase lherzolite and dunite.

orthopyroxene. At the margin of orthopyroxenes, negative concentration gradient of Al_2O_3 and CaO are pronounced toward the periphery of the grains. The Cr_2O_3 content also decreases at the margin. In this case the Mg/Mg+Fe ratio is rather constant throughout the grains.

TEMPERATURE ESTIMATES

Temperatures of equilibration of chemically analyzed orthopyroxene-clinopyroxene pairs from the Horoman ultramafic rocks are summarized in Text-fig. 34. The temperatures were calculated for the core-core pairs of porphyroclastic primary grains, using the semi-empirical orthopyroxene-clinopyroxene geothermometer proposed by Wood and Banno (1973). Estimates for the same pairs using the Well's (1977) recalibration differ by 40° to 60°C from the temperatures obtained from the Wood and Banno's (1973) equation.

The equilibration temperatures mostly range between 900°C and 1,100°C, indicating subsolidus temperatures and that the Horoman ultramafic rocks were re-equilibrated in the upper mantle. Text-fig. 34 also shows the equilibration temperatures calculated for recrystallized orthopyroxene-clinopyroxene pairs. The temperatures for the Horoman pyroxene neoblasts range from 850°C to 1,000°C, which are considerably lower than those for primary porphyroclasts. It is expected from the estimates that the Horoman ultramsfic rocks were re-equilibrated under the above subsolidus conditions at which deformation and recrystallization proceeded.

Text-fig. 35 plots in K_D against $Y_{Cr} = Cr/Cr+Al+Fe^{3+}$ for the analyzed spinels that

$$K_D = \frac{X_{Mg}^{Ol} \; X_{Fe}^{Sp}}{X_{Fe}^{Ol} \; X_{Mg}^{Sp}}$$

lie on the chromite-spinel join with Y_{Cr} held constant at 0.05. The K_D values defined as were calculated for olivine-spinel pairs from the Horoman ultramafic series. The 700°C and 1,200°C isopleths in Text-fig. 35 are from Evans and Frost (1975). All of the olivine-spinel pairs are plotted in the area between 700°C and 1,000°C. The quilibration temperatures are considerably lower than those obtained from the orthopyroxene-clinopyroxene pairs. It is questionable whether the olivine-spinel pairs coexisted in equilibrium under the subsolidus conditions or not.

TECTONIC INTRUSION MODEL FROM THE UPPER MANTLE

Considering the foregoing petrographical and mineralogical conclusions and discussions, a tectonic intrusion model for the Horoman layered massif is proposed as follows (Text-fig. 36).

The Horoman ultramafic rocks existed primarily as solid phases in the upper mantle. The ultramafic solids trapped the residual magma in many pockets, as mentioned earlier. At that time the ultramafic solids of dunite and lherzolite compositions were

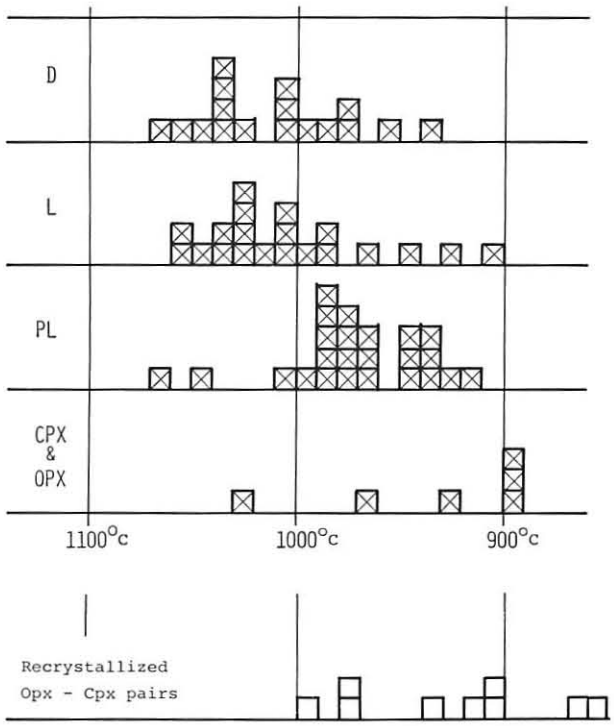

Text-fig. 34 Histogram of equilibration temperatures for Opx-Cpx parirs of porphyroclastic primary grains (box with cross) and recrystallized grains (open box) of the Horoman ultramafic massif. Calculation by the Opx-Cpx geothermometer (Wood and Banno, 1973).

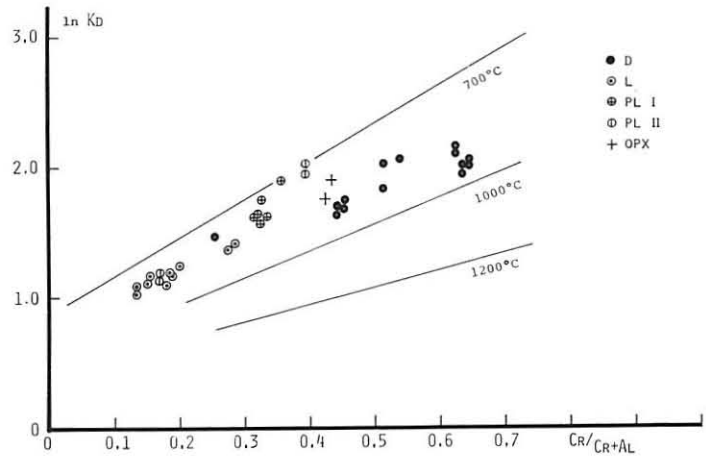

Text-fig. 35 In K_D vs. Cr/Cr+Al plots showing the reequilibration temperatures for the Horoman Ol-Sp pairs. 700°C and 1,200°C isopleths by Evans and Frost (1975).

completely consolidated, whereas those of plagioclase lherzolite probably possessed an interstitial liquid among the solid phases. The residual and interstitial magmas later crystallized into gabbroic phases, resulting in the gabbro I and II and the gabbroic seams in the plagioclase lherzolite I and II.

The equilibration temperatures ranging from 900°C to 1,100°C, obtained by calculations using the orthopyroxene-clinopyroxene geothermometer, were primarily frozen under the subsolidus conditions in the Upper mantle at that time.

Following the primary conditions, deformation and recrystallization took place in the solid parts of the mantle. The primary minerals were strongly strained and elongated into coarse, deformed grains with many kink bands. A large amount of olivine and pyroxene neoblasts were formed by inter- and intracrystalline recrystallization of primary grains which were also modified into porphyroclasts. The layered sequence of the Horoman massif is considered to have formed at that time by a gliding movement of the solid mantle with small magma pockets, and then a fragment of the mantle was pulled apart from the mantle and intruded into the Earth's crust. Strong concentratins of (100) crystallographic axis of olivine parallel to the lineations, reported by Niida (1975), were also formed. The temperatures estimated for the recrystallized pyroxene pairs, ranging between 850° and 1,000°C, indicated that the ultramafic solid phases were re-equilibrated under the conditions during the deformation and recrystallization processes.

As shown in Text-fig. 36, the re-equilibration in the upper mantle was followed by re-equilibration under the Earth's crust conditions. While the solid intrusion was uplifted tectonically toward the surface, intensive mylonitization probably occurred in the lower parts of the ultramafic sequence. Subsequently, the massif was affected by fracturing and weak serpentinization near the surface. Aggregations of talc and/or tremolite occurred along the fractures before the emplacement of the massif to the present position.

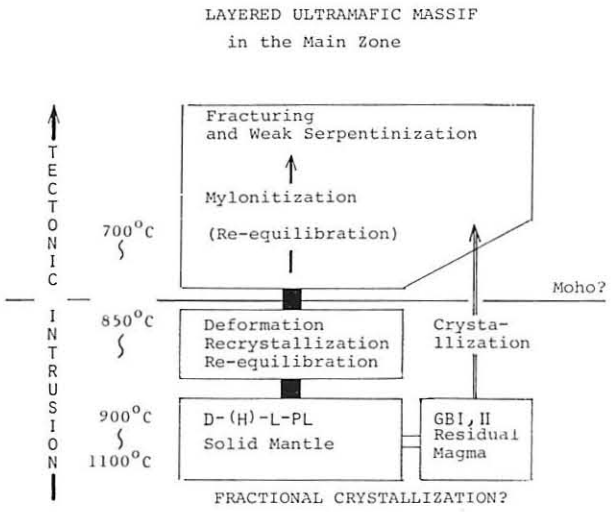

Text-fig. 36 Schematic diagram showing the tectonic development of the Horoman layered ultramafic massif from the upper mantle toward the surface.

Conclusions

1) The Horoman ultramafic massif represents an "alpine-type" ultramafic body which is a gently warped sheet more than 3,000 m in thickness. The massif exhibits a well-developed layered structure which consists of layers of dunite, lherzolite, plagioclase lherzolite, and a small amount of gabbro and pyroxenite. Two types of layering are distinguished; one has a conspicuous layered structure consisting of thin compositional layers in the Upper Zone of the massif, and the other is characterized by massive, thick, and gradational compositional layers in the Lower Zone. The massif is completely bounded by faults and shear zones. Evidence of contact metamorphim has not been found. The Horoman massif is regarded as a continuous body, because the sequence of the layering is traceable throughout the massif. Lineations show a constant direction of N15°E—S15°W throughout the massif. It is probable that the thick sheet was uplifted along the deep-seated thrust fault zone striking NW-SE, which passes through the northern side of the massif, and that the completely solidified sheet was thrust up to the southwest with gentle inclination to near the present level.

2) The textures of the Horoman ultramafic rocks are characterized by deformation, recrystallization and mylonitization. Except for the gabbroic rocks, no primary igneous texture is found in the ultramafic rocks of the massif. Three different types of olivine are classified from the grain size, grain shape, and mode of deformation. The first type is a coarse, deformed olivine which is considered to be porphyroclastic primary grains with many kink bands. The second type is a polygonal olivine showing a typical mosaic texture which was most probably formed by recrystallization. The last one is a fine olivine which was produced by mylonitization. Strongly strained grains of the olivine porphyroclasts are often found in the Lower Zone of the massif. Moreover, monomineralic seams of the fine olivine characteristically develop near the lowest parts of the massif. The textural development after consolidation of the massif can be considered as follows; formation of layered sequence → deformation of primary coarse olivine and recrystallization into polygonal olivine → mylonitization → fracturing and weak serpentinization.

3) The Lower Zone of the Horoman massif is made up mainly of the thick layers of dunite, lherzolite, and plagioclase lherzolite. The layering is characterized by a regular repetition in the layered sequence. On the other hand, the Upper Zone is characterized by development of the gabbroic rocks and a conspicuous layered structure, showing alternation of thin bands and layers of the plagioclase lherzolite, gabbro, and dunite. The cryptic layering of the Horoman massif shows a "symmetrical and wavy" pattern of gradual increase and decrease in Fe content of ferromagnesian silicates with the lithological change in the layered sequence. Futhermore, a consistent increase in Fe content of the minerals upward in the massif is also observed.

4) On the basis of chemical composition of the primary minerals the genesis of the Horoman massif can be explained by a successive fractional crystallization. The main sequence of the fractional crystallization resulted in the following series: dunite → lherzolite → plagioclase lherzolie → gabbro I. Another fractional crystallization sequence

which is recognized locally in the Upper Zone of the massif caused a continuous change from dunite to gabbro II. It seams likely that all the gabbroic rocks were formed by crystallization of residual liquids at the later stage. The gabbroic seams in the plagioclase lherzolite were also formed by crystallization of interstitial liquids. The residual liquid of the Horoman massif gradually changed from non-alkaline to alkaline with proceeding fractional crystallization.

5) The Horoman ultramafic rocks have been strongly modified by deep-seated deformation and recrystallization. Two different variation trends in chemical composition of primary pyroxenes can be traced; one is a primary crystallization trend which shows Fe-enrichment during proceeding of fractional crystallization, and the other is a re-equilibration trend which shows Al-, Ca-, and Cr- depletions at the margin. Step-scanning EPMA analyses revealed that the primary compositions show high and constant compositional plateaus at the core of the porphyroclastic primary grains.

6) The equilibration temperatures were calculated for the othopyroxene-clinopyroxene pairs of primary grains, using the pyroxene geothermometer proposed by Wood and Banno (1973). The temperatures range from 900° to 1,100°C. The temperature estimates for neoblastic recrystallized grains of pyroxene range between 850° and 1,000°C. The Horoman ultramafic rocks are considered to have been re-equilibrated under the above subsolidus conditions in the upper mantle where deformation and recrystallization occurred.

Acknowledgements

The present writer wishes to express his sincere thanks to Professor Y. Katsui of the Hokkaido University for kind guidance and encouragement during the study. He also wishes to express his appreciation to Emeritus Professors T. Ishikawa, M. Hunahashi, S. Hashimoto, K. Yagi, and Professor T. Bamba of the same university, and Professor K. Kizaki of the Ryukyu University for drawing his attention to this study and for their helpful advice. Special thanks are expressed to Dr. K. Onuma of the Tohoku University, Dr. Y. Oba of the Yamagata University, Dr. M. Komatsu of the Niigata University, Drs. T. Watanabe and Y. Yamaguchi of the Shimane University, Dr. K. Tazaki of the Okayama University, Prof. Y. Kuroda of the Shinshu University, Prof. S. Igi and Dr. T. Nagao of the Yamaguchi University, for their valuabale suggestions. He is grateful to Drs. K. Arita, S. Miyashita, and M. Yamamoto, and members of the "Research Group of Geotectonics in Hokkaido" for their helpful suggestions.

Acknowledgements must be made to Drs. K. Okumura, T. Soya, and H. Sato of the Geological Survey of Japan for their kind assistance with EPMA analysis and computer programming. Thanks are also due to Mrs. S. Yokoyama of the Hokkaido University for typing the manuscript and to Messrs. K. Moribayashi and T. Kuwajima of the same university for making thin sections. This study was financially supported by the Grant-in-Aid for Scientific Research from the Ministry of Education, Science and Culture of Japan.

References

Anastasiou, P. and Seifert, F., 1972. Solid solubility of Al_2O_3 in enstatite at high temperature and 1-5 kb water pressure. *Contr. Mineral. Petrol.*, 34: 272-287.

Aoki, K. and Matsumoto, H., 1959. On kaersutite from the Iki island, Nagasaki prefecture. *J. Japan. Assoc. Min. Pet. Econ. Geol.*, 43: 248-253 (in Japanese with English abstract).

Arima, M., Onuma, K. and Yagi, K., 1975. The solubility of Al_2O_3 in enstatite and the phase equilibria in the system $MgSiO_3$-$MgAl_2SiO_6$ at high temperature and pressure. *Proc. 4th Intern. Conf. on High Pressure*: 216-220.

AvéLallemant, H.G. and Carter, N.L., 1970. Syntectonic recrystallization of olivine and mode of flow in the upper mantle. *Geol. Soc. Amer. Bull.*, 81: 2203-2220.

Bamba, T., 1953. Studies on spinels associated with the ultramafic rocks in Hokkaido. *Jour. Geol. Soc. Japan.*, 59: 122-128 (in Japanese with English abstact).

Barberi, F., Bizouard, H. and Varet, J., 1971. Nature of the clinopyroxenes and iron enrichment in alkalic and transitional basaltic magmas. *Contr. Mineral. Petrol.*, 33: 93-107.

Boudier, F. and Nicolas, A., 1977. Structural controls on partial melting in the Lanzo peridotites. *Bull. Oregon St. Dept. Geol. Min.*, 96: 63-78.

Boyd, F.R. and England, J.L., 1964. The system enstatite-pyrope. *Carnegie Inst. Wash. Year Book*, 63: 157-161.

Carmichael, I.S.E., Nicholls, J.E., and Smith, A.L., 1970. Silica activity in igneous rocks. *Amer. Min.*, 55: 246-263.

Carswell, D.A., 1968. Picritic magma-residual dunite relationships in garnet peridotite at Kalskaret near Tafjord, South Norway. *Contr. Mineral. Petrol.*, 19: 97-124.

Carter, N.L., Raleigh, C.B., and DeCarli, P.S., 1968. Deformation of olivine in stony meteorites. *Jour. Geoph. Research*, 73: 5439-5461.

Carter, N.L. and AvéLallemant, H.G., 1970. High temperature flow of dunite and peridotite. *Geol. Soc. Amer. Bull.*, 81: 2181-2202.

Challis, G.A., 1965. The origin of New Zealand ultramafic intrusions. *J. Petrol.*, 6: 322-364.

Dawson, J.B. and Smith, J.V., 1973. Alkalic pyroxenite xenoliths from the Lashaine Volcano, northern Tanzania. *J. Petrol.*, 14: 113-131.

Dick, H.J.B., 1977. Partial melting in the Josephine peridotite I, the effect on mineral composition and its consequence for geobarometry and geothermometry. *Amer. Jour. Sci.*, 277: 801-832.

Dickey, J.S., 1970. Partial fusion products in alpine-type peridotites: Serrania de la Ronda and other examples. *Min. Soc. Amer., Special paper* 3: 33-49.

Dickey, J.S., Obata, M. and Suen, C.J., 1977. Partial fusion versus fractional crystallization: hypotheses for the differentiation of the Ronda ultramafic massif of southern Spain. *Bull. Oregon St. Dept. Geol. Min.*, 96: 79-89.

Ernst, W.G., 1978. Petrochemical study of lherzolitic rocks from the western Alps. *J. Petrol.*, 19: 341-392.

Evans, B.W. and Frost, B.R., 1975. Chrome-spinel in progressive metamorphism-preliminary analysis. *Geochim. Cosmochim. Acta*, 39: 959-972.

Gibb, F.G.F., 1973. The zoned clinopyroxenes of the Shiant Isles Sill, Scotland. *J. Petrol.*, 14: 203-230.

Green, D.H., 1964. The petrogenesis of the high-temperature peridotite intrusion in Lizard area, Cornwall. *J. Petrol.*, 5: 134-188.

Harada, J., Hunahashi, M., and Kobayashi, H., 1960. *Report on the peridotite complex of Apoi-dake, Hidaka.* Hokkaido Development Agency. (in Japanese).

Hashimoto, S., 1949. On the Poroshiri-dake plutonic complex, northern Hidaka mountains, Hokkaido. *Earth Sci.*, 1: 1-6.

Hashimoto, S., 1975. The basic plutonic rocks of the Hidaka metamorphic belt, Hokkaido. Part I. *Jour. Fac. Sci., Hokkaido Univ., Ser IV,* 16: 367-420.

Hess, H.H., 1960. Stillwater igneous complex, Montana. *Geol. Soc. Amer. Memoir* 80, 230 pp.

Himmelberg, G.R. and Loney, R.A., 1973. Petrology of the Vulcan Peak Alpine-type peridotite, southwestern Oregon *Geol. Soc. Amer. Bull.*, 84: 1585-1600.

Hirota, S., 1955. The features of plagioclase twinning in the gabbros and peridotites from the Horoman river district, southern Hidaka, Hokkaido. *Research Bull. Geol. Minerl. Institute, Tokyo Univ. of Education.*, 4: 47-56 (in Japanese with English abstract).

Hunahashi, M., 1941. Geology and petrology of the Horoman district, Hidaka. *Graduation thesis of Dept. of Geol. & Miner., Hokkaido Univ.*, no. 90 (manuscript in Japanese).

Hunahashi, M. and Hashimoto, S., 1951. Geology of the Hidaka zone, Hokkaido. *Monogr. Assoc. Geol. Collab. Japan*, no. 6 (in Japanese).

Hunahashi, M. and Igi, S., 1956. Explanatory text of the geological map of Japan "Horoizumi" (scale 1:50,000). Geol. Surv. Japan (in Japanese with English abstract).

Hunahashi, M., 1957. Alpine orogenic movement in Hokkaido, Japan. *Jour. Fac. Sci., Hokkaido Univ., Ser. IV*, 9: 415-467.

Igi, S., 1953. Petrographical studies on the peridotite in the Horoman region at the southern end of the Hidaka mountain range, Hokkaido. *Jour. Geol. Soc. Japan*, 59: 111-121 (in Japanese with English abstract).

Inomata, M. and Tazaki, K., 1974. Phlogopite and Ti-pargasite bearing ultramafic rocks from the Mikabu zone, central Japan. *J. Japan. Assoc. Min. Pet. Econ. Geol.*, 69: 205-214.

Irvine, T.N., 1967. The Duke Island ultramafic complex, southeastern Alaska. In: P.J. Wyllie (Editor) *Ultramafic and related rocks*, 84-97.

Irvine, T.N., 1974. Petrology of the Duke Island ultramafic complex, southern Alaska. *Geol. Soc. Amer., Memoir* 138: 1-240.

James, O.B., 1971. Origin and emplacement of the ultramafic rocks of the Emigrant Gap area, California. *J. Petrol.*, 12: 523-560.

Jan, M.Q. and Howie, R.A., 1981. The mineralogy and geochemistry of the metamorphosed basic and ultrabasic rocks of the Jijal Complex, Kohistan, NW Pakistan. *J. Petrol.*, 22: 85-126.

Komatsu, M. and Nochi, M., 1966. Ultrabasic rocks in Hidaka metamorphic belt, Hokkaido, Japan. I. Mode of occurrence of the Horoman ultrabasic rocks. *Earth Science*, 20: 21-29 (in Japanese with English abstract).

Komatsu, M., 1970. Petrological study of ultrabasic rocks in the Hidaka memamorphic belt, *Ph. D. thesis of Hokkaido Univ.*, (in Japanese).

Komatsu, M., Kimura, G. and Kiminami, K., 1981. Tectonics of Hokkaido, with special reference to the Hidaka Metamorphic Belt. In: I. Hara (Editor), *Tectonics of paired metamorphic belt.* Hiroshima, pp. 55-59.

Komatsu, M., Miyashita, S., Maeda, J., Osanai, Y. and Toyoshima, T., 1983. Disclosing of a deepest section of continental type crust up-thrust as the final event of collision of arcs in Hokkaido, north Japan. In: M. Hashimoto and S. Uyeda (Editors), *TERRAPUB*, Tokyo, pp. 149-165.

Kushiro, I., 1960. Si-Al relation in clinopyroxenes from igneous rocks. *Amer. Jour. Sci.*, 258: 548-554.

Lappin, M.A., 1967. Structural and petrofabric studies of the dunites of Almklovkalen, Nordfjord, Norway. In: P.J. Wyllie (Editor) *Ultramafic and related rocks*: Wiley, New York, 403-416.

Lauder, W.R., 1965. The geology of Dun Mountain, Nelson, New Zealand. Part 2 — The petrology, structure, and origin of the ultrabasic rocks. *N.Z. Geol. Geophys.*, 8: 475-504.

Leake, B.E., 1968. A catalog of analized calciferous and subcalciferous amphiboles together with their nomenclature and associated minerals. *Geol. Soc. Amer., Spec. Pap.* 98: 1-210.

LeBas, M.J., 1962. The role of aluminum in igneous clinopyroxenes with relation to their parentage. *Amer. Jour. Sci.*, 260: 267-288.

Loney, R.A., Himmelberg, G.R., and Coleman, R.G., 1971. Structure and petrology of the Alpine-type peridotite at Burro Mountain, California, U.S.A. *J. Petrol.*, 12: 245-309.

MacGregor, I.D., 1974. The system MgO-Al_2O_3-SiO_2: solubility of Al_2O_3 in enstatite for spinel and garnet peridotite composition. *Amer. Min.*, 59: 110-119.

Mercier, J.C.C. and Nicolas, A., 1975. Textures and fabrics of upper-mantle peridotites as illustrated by xenoliths from basalts. *J. Petrol.*, 16: 454-487.

Minato, M., Gorai, M., and Hunahashi, M. ed., 1965. *The geologic development of the Japanese islands.* Tsukiji-shokan, Tokyo.

Miyashita, S. and Maeda, J., 1978. The basic plutonic and metamorphic rocks from the northern Hidaka Metamorphic Belt, Hokkaido. *Monograph*, 21: 43-60 (in Japanese with English abstract).

Miyashita, S., 1983. Reconstruction of the ophiolite succession in the western zone of the Hidaka Metamorphic Belt, Hokkaido. *Jour. Geol. Soc. Japan*, 89: 69-86 (in Japanese with English abstract).

Möckel, L.R, 1969. The structural petrology of the garnet peridotite of Alpe Arami. *Leid. Geol. Mededel.*, 42: 61-130.

Mossman, D.J., 1973. Geology of the Greenhills ultramafic complex, Bluff peninsula, Southland, New Zealand. *Geol. Soc. Amer. Bull.*, 84: 39-64.

Murray, R.J., 1954. The Clinopyroxenes of the Garbh Eilean Sill, Shiant Isles. *Geol. Mag.*, 91: 17-31.

Nagasaki, H., 1962. Ultramafic body from the Horoman district, Hokkaido (abstract). *Jour. Geol. Soc. Japan*, 68: 406 (in Japanese).

Nagasaki, H., 1966. A layered ultrabasic complex at Horoman, Hokkaido, Japan. *Jour. Fac. Sci., Tokyo Univ.*, 16: 313-346.

Nash, W.P. and Wilkinson, J.F.G., 1970. Shonkin Sag Laccolith, Montana. I. Mafic minerals and estimates of temperature, pressrue, oxygen fugasity and silica activity. *Contr. Mineral. Petrol.*, 25: 241-269.

Nicolas, A., Bouchez, J.L., Boudier, F., and Mercier, J.C., 1971. Textures, structures and fabrics due to solid state flow in some European lherzolite. *Tectonophysics*, 12: 55-86.

Niida, K., 1974. Structure of the Horoman ultramafic massif of the Hidaka metamorphic belt in Hokkaido, Japan. *Jour. Geol. Soc. Japan*, 80: 31-44.

Niida, K., 1975. Phlogopite from the Horoman ultramafic rocks. *Jour. Fac. Sci., Hokkaido Univ., Ser. IV*, 16: 511-518.

Niida, K., 1975. Textures and olivine fabrics of the Horoman ultramafic rocks, Japan. *J. Japan Assoc. Min. Pet. Econ. Geol.*, 70: 265-285.

Niida, K. and Katoh, T., 1978. Ultramafic rocks in Hokkaido. *Monograph*, 21: 61-81 (in Japanese with English abstract).

Nochi, M. and Komatsu, M., 1967. Ultrabasic rocks in the Hidaka metamorphic belt, Hokkaido, Japan. II. Petrological relationships of the ultrabasic rocks and the olivine gabbro in the Uenzaru-Pankenushi area. *Earth Science*, 21: 11-26 (in Japanese with English abstract).

Obata, M., 1980. The Ronda peridotite: garnet-, spinel-, and pl-lherzolite facies and the P-T trajectories of a high-temperature mantle intrusion. *J. Petrol.*, 21: 533-572.

Ohdaira, Y., 1926. Geological and petrographical study in the Horoizumi district, Hidaka. *Jour. Geol. Soc. Japan*, 35: 105-147. (in Japanese).

Onuki, H., 1965. Petrochemical research on the Horoman and Miyamori ultramafic intrusions, North Japan. *Sci. Rept. Tohoku Univ., Ser. III*, 9: 217-276.

Onuma, K. and Arima, M., 1975. The join $MgSiO_3$-$MgAl_2SiO_6$ and the solubility of Al_2O_3 in enstatite at atmospheric pressure. *J. Japan. Assoc. Min. Pet. Econ. Geol.*, 7: 53-60.

Osanai, Y., Toyoshima, T. and Komatsu, M., 1981. Constitution of the Hidaka Metamorphic Belt; its metamorphism and structure. In: I. Hara (Editor), *Tectonics of paired metamorphic belt*. Hiroshima, pp. 11-17.

Presnall, D.C., 1969. The geometrical analysis of partial fusion. *Amer. Jour. Sci.*, 267: 1178-1194.

Ragan, D.M., 1963. Emplacement of the Twin Sisters dunite, Washington. *Amer. Jour. Sci.*, 261: 549-565.

Raleigh, C.B., 1965. Glide mechanisms in experimentally deformed minerals. *Science*, 150: 739-741.

Raleigh, C.B. 1967. Plastic deformation of upper mantle silicate minerals. *Geophys. J.R. Astr. Soc.*, 14: 45-49.

Raleigh, C.B., 1968. Mechanism of plastic deformation of olivine. *Jour. Geophys. Res.*, 73: 5391-5406.

Research Group of Peridotite Intrusion., 1967. Ultrabasic rocks in Japan. *Jour. Geol. Soc. Japan*, 73: 543-553.

Ross, M., Bence, A.E., Dwornik, E.J., Clark, J.R., Papike, J.J., 1970. Lunar clinopyroxenes: chemical composition, structural state, and texture. *Science* 167: 628-630.

Ruckmick, J.C. and Noble, J.A., 1959. Origin of the ultramafic complex at Union Bay, southeastern Alaska. *Bull. Geol. Soc. Amer.*, 70: 981-1018.

Shervais, J.W., 1979. Thermal emplacement model for the Alpine Lherzolite massif at Balmuccia, Italy. *J. Petrol.*, 20: 795-820.

Smith, C.H., 1958. Bay of Islands igneous complex, western Newfoundland. *Canada Geol. Survey Mem.*, 290: 1-132.

Smith, C.H. and Kapp, H.E., 1963. The Muskox intrusion. *Miner. Soc. Amer. Spec. Paper*, 1: 30-35.

Sweatman, T.R. and Long, J.V.P., 1969. Quantitative electronprobe microanalysis of rock forming minerals. *J. Petrol.*, 10: 332-379.

Takeuchi, N., 1937. Report of mineral resources in the Horoizumi and Samani district, Hidaka. *Miner. Resource Rept., Hokkaido Indust. Res. Inst.*, no. 67 (in Japanese).

Tazaki, K., Ito, E., and Komatus, M., 1972. Experimental study on a pyroxene-spinel symplectite of high pressures and temperatures. *Jour. Geol. Soc. Japan*, 78: 347-354.

Tazaki, K. and Inomata, M., 1974 Phlogopites and coexisting pargasites in wehrlite from the northern Kanto mountains, central Japan. *Papers Inst. Thermal Spring Research, Okayama Univ.*, 43: 1-13 (in Japanese with English abstract).

Tenpaku, T., 1967. On the plagioclase feldspar in the peridotite mass in the Horoman area, Hokkaido. *Earth Science*, 21: 10-13 (in Japanese).

Thayer, T.P., 1960. Some critical differences between Alpine-type and stratiform peridotite-gabbro complexes. *21st. Intern. Geol. Congr., Copenhagen Rept*. 13: 247-259.

Verhoogen, J., 1962. Distribution of titanium between silicates and oxides in igneous rocks. *Amer. Jour. Sci.*, 260: 211-220.

Wager, L.R., Brown, G.M., and Wadsworth, W.J., 1960. Types of igneous cumulates. *J. Petrol.*, 1: 73-85.

Wager, L.R. and Brown, G.M., 1967. *Layered igneous rocks*. Oliver and Boyed, Edinburgh.

Wager, L.R., 1968. Rhythmic and cryptic layering in mafic and ultramafic plutons. In: H.H. Hess. and A. Poldervaart (Editors) *Basalts*, Vol. 2.

Walcott, R.I., 1968. Geology of the Red Hill complex, Nelson, New Zealand. *Trans. R. Soc. N.Z., Earth Science*, 7: 57-88.

Wells, P.R.A., 1977. Pyroxene thermometry in simple and complex systems. *Contr. Mineral. Petrol.*, 62: 129-139.

Wilkinson, J.F.G., 1957. The clinopyroxenes of a differentiated teschenite sill near Gunnedah, New South Wales. *Geol. Mag.*, 94: 123-134.

Wilkinson, J.F.G., 1961. Some aspects of the calciferous amphiboles, Oxyhornblende, kaersutite and barkevikite. *Amer. Min.*, 46: 340-354.

Wilshire, H.G., Calk, L.C. and Schwarzman, E.C., 1971. Kaersutite — a product of reaction between pargasite and basanite at Dish Hill, California. *Earth. Planet. Sci. Letters.*, 10: 281-284.

Wilshire, H.G. and Trask, N.J., 1971. Structural and textural relationships of amphibole and phlogopite in peridotite inclusions, Dish Hill, California. *Amer. Miner.*, 56: 240-255.

Wood, B.J. and Banno, S., 1973. Garnet-orthopyroxene and orthopyroxene-clinopyroxene relationships in simple and complex systems. *Contr. Mineral. Petrol.*, 42: 109-124.

Yagi, K., 1953. Petrochemical studies on the alkalic rocks of the Morotu District, Sakhalin. *Bull. Geol. Soc. Amer.*, 64: 769-810.

Yagi, K. and Onuma, K., 1967. The join $CaMgSi_2O_6$ and its bearing on the titanaugites. *Jour. Fac. Sci., Hokkaido Univ., Ser. IV*, 13: 463-483.

Yamaguchi, Y. and Tomita, K., 1970. Clinoenstatite as an exsolution phase in diopside. *Mem. Fac. Sci., Kyoto Univ.*, 37: 174-180.

Yamane, S., 1911. Report of mineral resources in the southern area of Hidaka and the Hiroo district of Tokachi, Hokkaido. *Rept. Miner. Resources in Japan, Geol. Serv. Japan*, no. 4 (in Japanese).

Young, C., 1969. Dislocations in the deformation of olivine. *Amer. Jour. Sci.*, 267: 841-852.

(Manuscript received on Oct. 31, 1983; revised and accepted on Nov. 18, 1983)